

1 **Decadal Evolution of Aerosol-Mediated Ozone Responses in Eastern**
2 **China under Clean Air Actions and Carbon Neutrality Policies**

3 Yasong Li^{1,3}, Chen Li², Yaoyu Li¹, Tijian Wang^{3*}, Mengmeng Li³, Yawei Qu⁴, Hao Wu⁵, Min Xie⁶, Yanjin
4 Wang¹

5 1. *College of Environmental Economics, Henan Finance University, Zhengzhou, 450046, China*

6 2. *School of Energy and Chemical Engineering, Tianjin Renai College, Tianjin, 301636, China*

7 3. *School of Atmospheric Sciences, Nanjing University, Nanjing, 210023, China*

8 4. *College of Intelligent Science and Control Engineering, Jinling Institute of Technology, Nanjing, 211112, China*

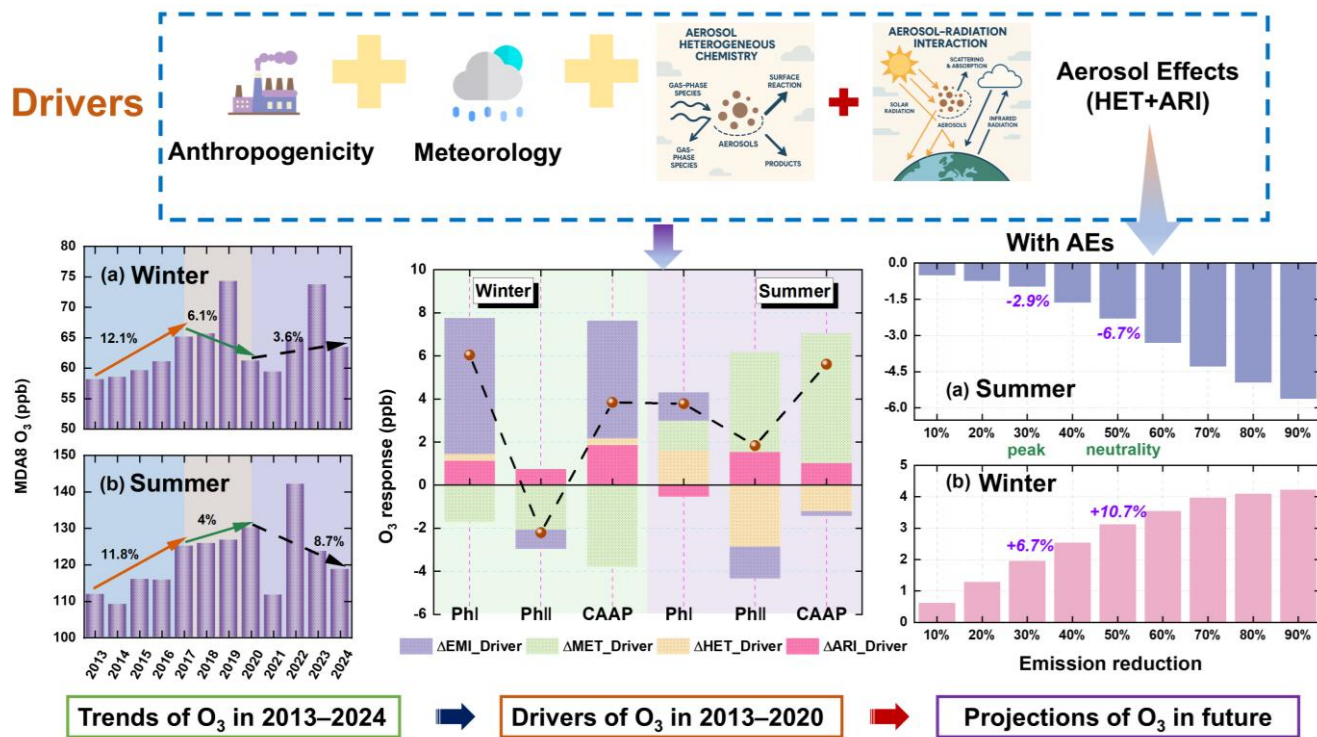
9 5. *Key Laboratory of Transportation Meteorology of China Meteorological Administration, Nanjing Joint Institute for*
10 *Atmospheric Sciences, Nanjing, China*

11 6. *School of Environment, Nanjing Normal University, Nanjing 210023, China*

12 **Correspondence to:** Tijian Wang (tjwang@nju.edu.cn)

13 **Abstract:**

14 Despite substantial reductions in $\text{PM}_{2.5}$ and other pollutants, ozone (O_3) in eastern China has increased over the past
 15 decade, yet the influence of aerosol processes—including aerosol–radiation interactions (ARI) and heterogeneous chemistry
 16 (HET)—on these trends remains insufficiently explored, particularly during Clean Air Action Plan (CAAP, Phase I: 2013–
 17 2017; Phase II: 2018–2020) and under carbon neutrality pathways. We applied a phase- and season-resolved WRF-Chem
 18 framework with explicit ARI and HET to quantify historical and projected O_3 changes in the Yangtze River Delta (YRD),
 19 linking aerosol effects with CAAP and carbon-neutrality pathways. We separate O_3 changes into those driven directly by
 20 anthropogenic emissions and meteorological variability, and those mediated by aerosol processes through ARI and HET. The
 21 results revealed that anthropogenic emissions and meteorological variability respectively dominated winter and summer O_3
 22 increases. Winter O_3 increases were dominated by ARI: large aerosol reductions enhanced solar radiation, temperature, and
 23 photolysis, resulting in a photochemical O_3 rise (+1.14 (+0.74) ppb in Phase I (II)). Summer O_3 was more sensitive to HET.
 24 In Phase I, aerosol decreases weakened heterogeneous radical uptake, enhancing O_3 formation (+1.62 ppb). In Phase II,
 25 however, the net HET effect reversed sign (−2.86 ppb), driven by shifts in multiple heterogeneous pathways—including
 26 changes in radical uptake, HONO and N_2O_5 chemistry, and aerosol liquid water—rather than radical scavenging alone.
 27 Accounting for aerosol effects (AEs=ARI+HET), reductions in $\text{PM}_{2.5}$ and NO_x increased O_3 , while VOCs reductions
 28 consistently lowered O_3 in both seasons. Under carbon peaking and neutrality scenarios with AEs, winter O_3 increased by 6.7%
 29 and 10.7%, whereas summer O_3 decreased by 2.9% and 6.7%, highlighting seasonally contrasting responses. These results
 30 underscore the necessity of explicitly accounting for multi-path aerosol– O_3 interactions in both near-term air quality
 31 management and long-term climate mitigation to prevent unintended trade-offs and maximize co-benefits.

32 **Graphical Abstract:**

34 1. Introduction

35 Over the last decade, a series of landmark policy initiatives—such as the Air Pollution Prevention and Control Action
36 Plan (Phase I: 2013–2017), the Three-Year Blue Sky Protection Campaign (Phase II: 2018–2020), and the subsequent dual-
37 carbon strategy—have driven substantial and persistent declines in PM_{2.5} concentrations across China's major urban clusters
38 (Geng et al., 2024; Zhai et al., 2019). However, in sharp contrast to these successes, ground-level O₃ have continued to rise,
39 particularly in economically developed regions such as Beijing-Tianjin-Hebei (BTH, (Zhao et al., 2023; Dai et al., 2023)), the
40 Yangtze River Delta (YRD, (Li et al., 2023; Hu et al., 2025)), and the Pearl River Delta (PRD, (Chen et al., 2020)). For example,
41 Yan et al. (2024) reported that the annual mean maximum daily 8-hour average (MDA8) O₃ in major Chinese cities increased
42 from 106.0 $\mu\text{g m}^{-3}$ in 2013 to 131.1 $\mu\text{g m}^{-3}$ in 2022, with the most pronounced growth observed in the BTH and YRD regions.
43 The emerging decoupling between PM_{2.5} and O₃ trends underscores the growing complexity of air pollution control in China,
44 suggesting that conventional precursor-oriented mitigation strategies may be insufficient to address secondary pollutants
45 formed through nonlinear atmospheric processes. The increasing frequency and intensity of O₃ pollution episodes not only
46 pose serious risks to human health and ecosystems (Liu et al., 2018; Li et al., 2020b) but also diminish the co-benefits of PM_{2.5}
47 mitigation. As China advances toward its goal of carbon neutrality, elucidating the mechanisms behind this counterintuitive
48 O₃ rise has become both a scientific imperative and a policy priority.

49 Extensive research has identified anthropogenic emissions and meteorological variability as the two dominant drivers of
50 observed O₃ increases (Ma et al., 2023a; Sun et al., 2019; Shao et al., 2024; Ni et al., 2024), particularly during the early stages
51 of the CAAP. For instance, Dang et al. (2021) used the GEOS-Chem model to show that during the summer of 2012–2017,
52 meteorological changes accounted for 49% of the O₃ increase in the BTH region and 84% in the YRD, while emission changes
53 explained 39% and 13%, respectively. Recent efforts combining numerical modeling with machine learning have further
54 highlighted the critical roles of solar radiation and temperature, especially during the COVID-19 lockdown. Zhang et al. (2025)
55 attributed approximately 94% of the summer O₃ increase in the Hangzhou Bay area from 2019 to 2022 to meteorological
56 influences, noting a growing dominance of meteorological drivers over emission-related factors. In addition, innovative
57 metrics such as the O₃-specific emission–meteorology index (EMI/O₃) have been proposed to quantify these contributions,
58 revealing that summer O₃ increases in cities like Beijing and Shanghai were largely governed by volatile organic compound
59 (VOCs) emissions and meteorological shifts (Lu et al., 2025).

60 Beyond emissions and meteorology, aerosol effects (AEs) have emerged as important, though often overlooked, regulators
61 of surface O₃. Aerosols influence O₃ formation through two principal mechanisms: aerosol–radiation interaction (ARI), which
62 alter photolysis rates and boundary layer dynamics, and heterogeneous chemistry (HET), which removes hydroperoxy (HO₂)
63 radical and suppresses O₃ formation (Li et al., 2025; Li et al., 2024b; Li et al., 2019a; Gao et al., 2018). As aerosol loading has

64 substantially declined under clean air policies, the magnitudes and directions of these mechanisms may have shifted. For
65 instance, Yu et al. (2019) found that reductions in PM_{2.5} contributed to approximately 22% of the observed O₃ increase in the
66 YRD during 2013–2017. Yang et al. (2024) quantified a 0.81 ppb increase in summer O₃ linked to the weakening of ARI under
67 lower aerosol conditions. Previous analyses indicated that diminished aerosol modulation of photochemistry through ARI,
68 photolysis rate suppression, and heterogeneous reactions jointly contributed to a 22.2%–57.3% enhancement in O₃ growth
69 between 2014 and 2020 (Li et al., 2024a). Similarly, Liu et al. (2023a) identified weakened HET as the dominant mechanism
70 behind O₃ increases across both phases of the CAAP. Moreover, precursor–O₃ relationships are strongly modulated by
71 background aerosol levels, further emphasizing the need to assess O₃ responses under evolving aerosol conditions to ensure
72 the effectiveness of co-control strategies. Anthropogenic emissions and meteorological variability act as external drivers that
73 directly regulate precursor concentrations, atmospheric chemical regimes, and transport processes. In contrast, ARI and HET
74 represent aerosol-mediated mechanisms that reshape the photochemical environment by altering photolysis rates and radical
75 budgets. These aerosol-driven mechanisms determine the extent to which surface O₃ responds to precursor (particularly NO_x)
76 reductions or meteorological perturbations. This conceptual framework underpins our separation of O₃ changes into externally
77 driven components and aerosol-modulated components in this study.

78 Despite increasing recognition of the role of aerosols in modulating surface O₃, several critical knowledge gaps remain.
79 Most existing studies tend to isolate either ARI or HET rather than evaluate their combined and potentially synergistic effects.
80 Additionally, few investigations adopt a phase- and season-resolved framework aligned with policy implementation timelines,
81 and even fewer consider long-term projections under carbon neutrality pathways. Furthermore, the spatial heterogeneity and
82 nonlinear chemical responses of O₃ under dynamic aerosol environments remain poorly characterized, particularly in densely
83 populated and industrialized regions like the YRD. To address these gaps, this study employs an improved WRF-Chem
84 modeling framework to conduct a comprehensive, phase-, season-, and mechanism-resolved assessment of AEs in the YRD
85 from 2013 to 2024. By explicitly disentangling the effects of ARI and HET and integrating them with historical emission
86 changes, meteorological variability, and future carbon neutrality–driven mitigation scenarios, we aim to systematically
87 quantify the drivers of past O₃ trends and predict their future trajectories. Furthermore, we assessed the responses of O₃ to
88 reductions in individual precursors (PM_{2.5}, NO_x, VOCs, NH₃, and SO₂), thereby elucidating the conditions under which
89 synergistic air quality and climate co-benefits can be most effectively realized. These results provide a scientific basis for the
90 development of region-specific and seasonally adaptive O₃ mitigation strategies that are consistent with China’s dual objectives
91 of air pollution control and carbon neutrality.

92 **2. Methodology**

93 **2.1 Model and dataset**

94 To diagnose the mechanisms governing surface O₃ variability over eastern China under the Clean Air Action Plan (CAAP),
95 we applied an improved configuration of the Weather Research and Forecasting model coupled with Chemistry (WRF-Chem,
96 version 3.7.1, (Grell et al., 2005)). The analysis focused on two major implementation stages of the CAAP (Phase I and Phase
97 II), with the objective of disentangling the relative contributions of emission controls, meteorological variability, and aerosol-
98 mediated processes to long-term O₃ changes. Particular attention was devoted to two key aerosol effects (ARI and HET) and
99 their roles in modulating O₃ trends. In addition, sensitivity experiments were conducted to quantify O₃ responses to precursor
100 emission reductions, and to evaluate future surface O₃ behavior under carbon neutrality-oriented emission pathways while
101 explicitly accounting for combined aerosol effects (ARI + HET). Building upon our previous modeling framework, the WRF-
102 Chem setup largely followed configurations documented in earlier studies (Li et al., 2024a; Li et al., 2024b), with targeted
103 enhancements to address the objectives of this work. A three-tier nested domain system was implemented, encompassing East
104 Asia as the outermost domain, eastern China as the intermediate domain, and the YRD as the innermost domain (Figure S1).
105 Biogenic emissions were calculated online using the Model of Emissions of Gases and Aerosols from Nature (Guenther et al.,
106 2006). Numerical simulations were performed for January and July to characterize representative winter and summer
107 conditions, respectively. Each seasonal simulation covered a five-week period (December 29 to February 1 for winter, and
108 June 28 to August 1 for summer), with the initial three days excluded to allow for model spin-up and chemical equilibration.
109 Beyond the seasonal analyses, the decadal evolution of maximum daily 8-hour average (MDA8) O₃ over the YRD during
110 2013–2024 was systematically examined for both seasons. Detailed information about the spatial distribution and technical
111 characteristics of the monitoring stations and model configuration have been reported in our previous studies (Li et al., 2024a).

112 **2.2 Aerosol effects enhancement**

113 This work provided a comprehensive evaluation of aerosol-mediated influences on surface O₃ variability within the dual
114 context of China's CAAP and prospective carbon neutrality pathways. Two representative aerosol-related processes (ARI and
115 HET) were explicitly represented in the WRF-Chem modeling system to account for the coupled physical and chemical
116 pathways through which aerosols regulate O₃ formation. The formulation, implementation, and performance evaluation of
117 these processes followed the methodologies established in our earlier studies and are only briefly outlined here for
118 completeness (Li et al., 2024b). Within this framework, ARI modulated O₃ concentrations through two primary mechanisms.
119 First, aerosols attenuated incoming solar radiation, thereby influencing photolysis frequencies through light extinction. Second,
120 aerosols perturbed meteorological conditions by altering radiative fluxes, giving rise to aerosol–radiation feedbacks (ARF).
121 While ARF was natively supported in the standard WRF-Chem configuration, the default Fast-J photolysis scheme did not

122 dynamically account for aerosol optical properties, which led to the omission of aerosol extinction effects on photolysis rates.
123 To overcome this deficiency, a customized coupling interface was implemented to link prognostic aerosol optical parameters—
124 such as scattering and absorption coefficients—to the Fast-J module. This modification allowed aerosol optical depth to be
125 calculated online and enabled photolysis rates to respond consistently to the evolving spatial and temporal distributions of
126 aerosols.

127 Heterogeneous chemistry exerts complex influences on O_3 formation by altering radical budgets, modifying reactive
128 nitrogen cycling, and changing aerosol-phase reaction rates. In the enhanced WRF-Chem, HET is represented through multiple
129 pathways on dust and black carbon surfaces, including (1) heterogeneous uptake of HO_2 , OH , NO_2 , and NO_3 ; (2) nighttime
130 N_2O_5 hydrolysis to $2HNO_3$; (3) heterogeneous formation of $HONO$ from NO_2 uptake on carbonaceous aerosols; (4) SO_2 and
131 H_2SO_4 heterogeneous oxidation; and (5) direct O_3 uptake on dust and black carbon surfaces. These processes collectively
132 modify photolysis-driven radical initiation and NO_x partitioning. Therefore, the net HET effect reflects the balance among
133 several aerosol-mediated pathways rather than a single mechanism. The heterogeneous reactions considered in this study,
134 together with their corresponding uptake coefficients (γ), were summarized in Table S1. Key parameters, including uptake
135 coefficients, aerosol surface area densities, and photolysis scaling factors, followed values that had been validated in our
136 previous modeling studies (Li et al., 2024b). The enhanced WRF-Chem system had been systematically assessed in earlier
137 work and was demonstrated to realistically reproduce meteorological fields, aerosol characteristics, and trace gas
138 concentrations in China, with particularly robust performance in YRD (Qu et al., 2023; Li et al., 2018).

139 **2.3 Numerical experimental designs**

140 To disentangle the respective and combined influences of anthropogenic emission changes, meteorological variability,
141 and aerosol-related processes on surface O_3 , three groups of numerical experiments were designed within the enhanced WRF-
142 Chem modeling framework (Table 1).

143 1) SET1: Historical Attribution Simulations (2013–2020).

144 The first set of simulations was conducted to identify the dominant drivers of O_3 variability during two major stages of
145 CAAP, referred to as Phase I and Phase II. In total, 11 simulations were performed to isolate the effects of emission changes,
146 meteorological variability, and aerosol-related mechanisms. To quantify the impact of anthropogenic emission changes alone,
147 three simulations were conducted using fixed meteorological conditions from 2020, with all aerosol-related effects disabled
148 (13E20M_NOALL, 17E20M_NOALL, and 20E20M_NOALL). Differences among these simulations represented the net O_3
149 response to emission evolution in the absence of aerosol feedbacks and meteorological variability. The contribution of
150 meteorological variability was assessed through an additional set of simulations using fixed anthropogenic emissions from
151 2013 while varying meteorological conditions (2013, 2017, and 2020). Aerosol-related processes were excluded in these runs
152 (13E13M_NOALL, 13E17M_NOALL, and 13E20M_NOALL), and the resulting differences quantified the meteorology-

153 driven component of O_3 changes. To evaluate aerosol effects (AEs), three parallel simulations were conducted for each
154 emission year (2013, 2017, and 2020): (i) with all aerosol-related processes enabled (AEs), (ii) with heterogeneous chemistry
155 disabled (NOHET), and (iii) with all aerosol effects turned off (NOALL). Pairwise comparisons among these simulations (e.g.,
156 AEs-NOHET, NOHET-NOALL, and AEs-NOALL) allowed the individual contributions of heterogeneous chemistry (HET),
157 aerosol-radiation interactions (ARI), and their combined effects to be quantified. For example, the difference between
158 20E20M_AEs and 20E20M_NOHET isolated the HET contribution under 2020 emission conditions, whereas the comparison
159 between 20E20M_NOHET and 20E20M_NOALL represented the ARI effect. This analytical framework was applied
160 consistently across all emission years to characterize phase-resolved aerosol influences on O_3 trends. A schematic illustration
161 of the experimental design and the associated O_3 responses was provided in Figure 1.

162 2) SET2: Single-Precursor Sensitivity Experiments (2020 baseline).

163 The second group of simulations was designed to examine the nonlinear responses of O_3 to individual precursor emission
164 controls under active aerosol effects. All experiments were based on the 2020 anthropogenic emissions inventory. For each
165 simulation, emissions of one precursor (primary PM_{2.5}, NOx, volatile organic compounds (VOCs), SO₂, or NH₃) were reduced
166 by 25% and 50%, while emissions of the remaining species were held constant. Reductions in primary PM_{2.5} included both
167 black carbon (BC) and organic carbon (OC).

168 3) SET3: Multi-Pollutant Co-Reduction Experiments (Future Scenarios).

169 The third set of experiments explored potential O_3 responses under future emission mitigation pathways aligned with
170 China's carbon peaking and carbon neutrality objectives. Coordinated reductions in all major anthropogenic emissions were
171 applied, guided by the mid- and long-term projections reported by Cheng et al. (2021), who assessed China's air quality
172 evolution under dual-carbon strategies. Their analysis suggested that anthropogenic emissions will decrease by approximately
173 26%–32% by 2030 relative to 2020 levels, followed by a slower reduction pace thereafter, reaching a maximum decline of
174 about 31% by 2060 compared to 2030. Based on these projections, two representative reduction levels—30% and 50%—were
175 selected to approximate emission conditions corresponding to the carbon peaking (2030) and carbon neutrality (2060) targets,
176 respectively. To further characterize the nonlinear O_3 response under increasingly stringent mitigation, a series of additional
177 co-control scenarios spanning 10%, 20%, 40%, 60%, 70%, 80%, and 90% reductions was implemented. Across all future
178 experiments, emissions of primary PM_{2.5}, NOx, VOCs, SO₂, and NH₃ were scaled down proportionally, reflecting a coordinated
179 multi-pollutant mitigation framework. Aerosol-related processes were consistently enabled in all simulations to preserve
180 realistic aerosol– O_3 feedbacks.

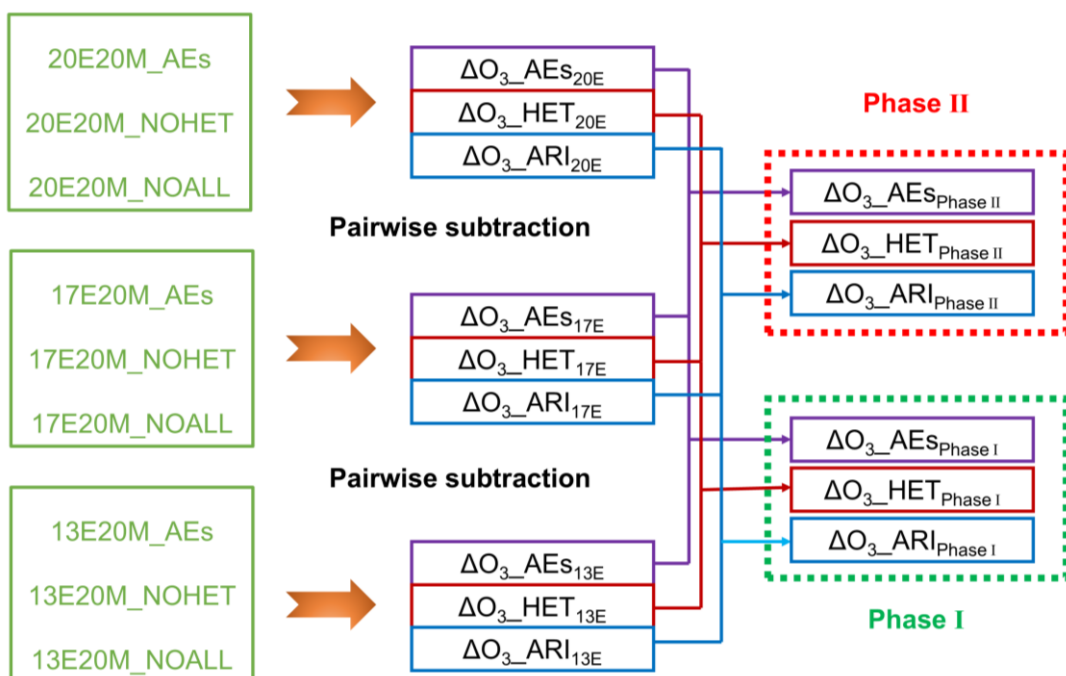
181 **Table 1** Overview of WRF-Chem numerical experiments.

Scenario sets	Scenario ID	Anthropogenic emissions	Meteorology	HET ^a	ARI ^b
---------------	-------------	-------------------------	-------------	------------------	------------------

	20E20M_AEs			✓	✓
	20E20M_NOHET	2020		✗	✓
	20E20M_NOALL			✗	✗
	17E20M_AEs			✓	✓
	17E20M_NOHET	2017	2020	✗	✓
SET1	17E20M_NOALL			✗	✗
	13E20M_AEs			✓	✓
	13E20M_NOHET	2013		✗	✓
	13E20M_NOALL			✗	✗
	13E13M_NOALL	2013	2013	✗	✗
	13E17M_NOALL	2013	2017	✗	✗
	CUT_PM _{2.5} _25/50	25 (50) % reduction in PM _{2.5} in 2020			
SET2	CUT_NOx_25/50	25 (50) % reduction in NOx in 2020			
	CUT_VOCs_25/50	25 (50) % reduction in VOCs in 2020			
	CUT_NH ₃ _25/50	25 (50) % reduction in NH ₃ in 2020			
	CUT_SO ₂ _25/50	25 (50) % reduction in SO ₂ in 2020			
	CUT_MEIC_10	10% reduction in 2020			
SET3	CUT_MEIC_20	20% reduction in 2020	2020	✓	✓
	CUT_MEIC_30	30% reduction in 2020			
	CUT_MEIC_40	40% reduction in 2020			
	CUT_MEIC_50	50% reduction in 2020			
	CUT_MEIC_60	60% reduction in 2020			
	CUT_MEIC_70	70% reduction in 2020			
	CUT_MEIC_80	80% reduction in 2020			
	CUT_MEIC_90	90% reduction in 2020			

182 HET^a: Heterogeneous chemistry (HET) was activated by setting the heterogeneous reaction switch to 1.
183 ARI^b: Aerosol–radiation interaction (ARI) was activated by turning on the aerosol–radiation feedback (aer_ra_feedback = 1)
184 and by linking aerosol optical properties to the photolysis calculation.

O₃ responses to aerosol effects in different emission phases



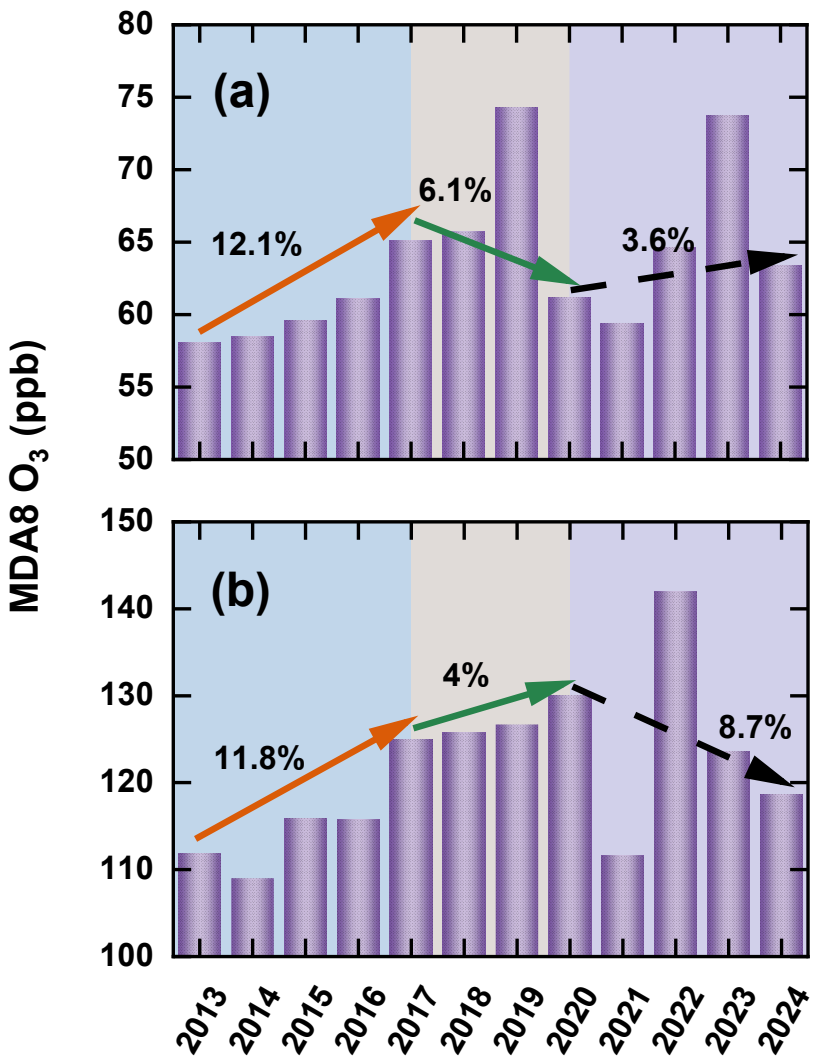
185 **Figure 1** Conceptual diagram illustrating the scenario design and the associated ozone responses to aerosol-mediated processes

187 during the CAAP phases. Note: HET=heterogeneous chemistry, ARI=aerosol-radiation interaction, AEs=aerosol effects
188 (HET+ARI). Scenario IDs such as “13E20M” refer to emission year 2013 with 2020 meteorology.

189 **2.4 Historical changes in emissions and observed O₃**

190 Interannual changes in six key species—SO₂, primary PM_{2.5}, BC, OC, NOx, and VOCs—at the provincial scale in the
191 YRD during 2013–2020 was presented in Figure S2. Over this period, emissions of most pollutants declined substantially,
192 with the exception of VOCs. Cumulatively, SO₂, primary PM_{2.5}, BC, OC, and NOx emissions were reduced by 69.7%, 46.9%,
193 40.4%, 38.0%, and 27.9%, respectively. During the first phase of the CAAP (Phase I), control strategies were predominantly
194 oriented toward particulate matter abatement. As a result, primary PM_{2.5}, BC, and OC emissions decreased markedly by 37.0%,
195 30.0%, and 27.3%, respectively. Concurrently, notable reductions were achieved for major gaseous precursors, with SO₂ and
196 NOx declining by 56.4% and 19.8%. In contrast, the absence of explicit VOCs-targeted measures during this stage led to a
197 7.1% increase in VOCs emissions (Li et al., 2019b). The second phase of the CAAP (Phase II) was characterized by a transition
198 toward more coordinated regulation of NOx and VOCs. Although emissions of SO₂, NOx, and PM_{2.5} continued to decrease,
199 the overall pace of reduction was slower than that observed in Phase I. Specifically, NOx and VOCs emissions declined by
200 7.4% and 4.6%, respectively. Nevertheless, when considering the entire 2013–2020 period, VOCs emissions in the YRD still
201 exhibited a net increase of 2.2%. From a spatial perspective, emission reductions were most pronounced in the northwestern
202 and central subregions of the YRD (Figure S3), a pattern that aligns with national emission reduction trends and is consistent
203 with previous regional assessments (Liu et al., 2023a; Yan et al., 2024).

204 In addition to modifying emissions, the CAAP brought about substantial changes in observed O₃. Figure 2 illustrated the
205 annual variation of the MDA8 O₃ in winter and summer across the YRD based on ground-based observations from 2013 to
206 2024. In winter, O₃ increased by approximately 7 $\mu\text{g m}^{-3}$ during 2013–2017, at an average annual growth rate of 3%. This trend
207 reversed during 2017–2020, with a decrease of 4 $\mu\text{g m}^{-3}$ (2% per year), followed by a modest increase of 2.2 $\mu\text{g m}^{-3}$ (0.91%
208 per year) between 2020 and 2024. In summer, O₃ rose by 13.2 $\mu\text{g m}^{-3}$ during 2013–2017, continued to increase by 4.9 $\mu\text{g m}^{-3}$
209 from 2017 to 2020, and then declined sharply by 11.4 $\mu\text{g m}^{-3}$ during 2020–2024. These results suggested that in the early phase
210 of clean air efforts, the insufficient control of O₃ precursors contributed to significant increases in both winter and summer O₃.
211 However, stronger VOCs and NOx control measures in recent years appeared to mitigate this upward trend. A particularly
212 sharp drop in O₃ between 2020 and 2021 was likely caused by a combination of intensified emission reductions and unusual
213 meteorological conditions (Yin et al., 2021). Overall, observed MDA8 O₃ in the YRD increased by 12.1% in winter and 11.8%
214 in summer during 2013–2017. In the subsequent periods (2017–2020 and 2020–2024), winter O₃ levels first declined and then
215 rebounded, while summer O₃ initially rose and then decreased. The underlying causes of these contrasting patterns were
216 explored in detail in the Results section. Note that this study did not focus on the spatial distribution of O₃ changes, as this
217 topic has already been extensively examined in previous literature (Hu et al., 2025; Zhao et al., 2023).



218
219 **Figure 2** Interannual variations in winter (a) and summer (b) MDA8 O₃ concentrations (ppb) across the YRD during 2013–
220 2024, derived from continuous ground-based measurements.

221 **3. Results and discussion**

222 The accuracy of simulated meteorological parameters and pollutant concentrations under scenario (20E20M_AEs) has
223 been thoroughly validated against ground-based observations in earlier work (Li et al., 2024a). As summarized in Table S2,
224 the model reasonably captures the magnitude, seasonal variability of PM_{2.5}, O₃, as well as the major features of temperature,
225 relative humidity, and wind speed. These results provide confidence in the model's ability to represent the atmospheric
226 conditions relevant to the subsequent analysis.

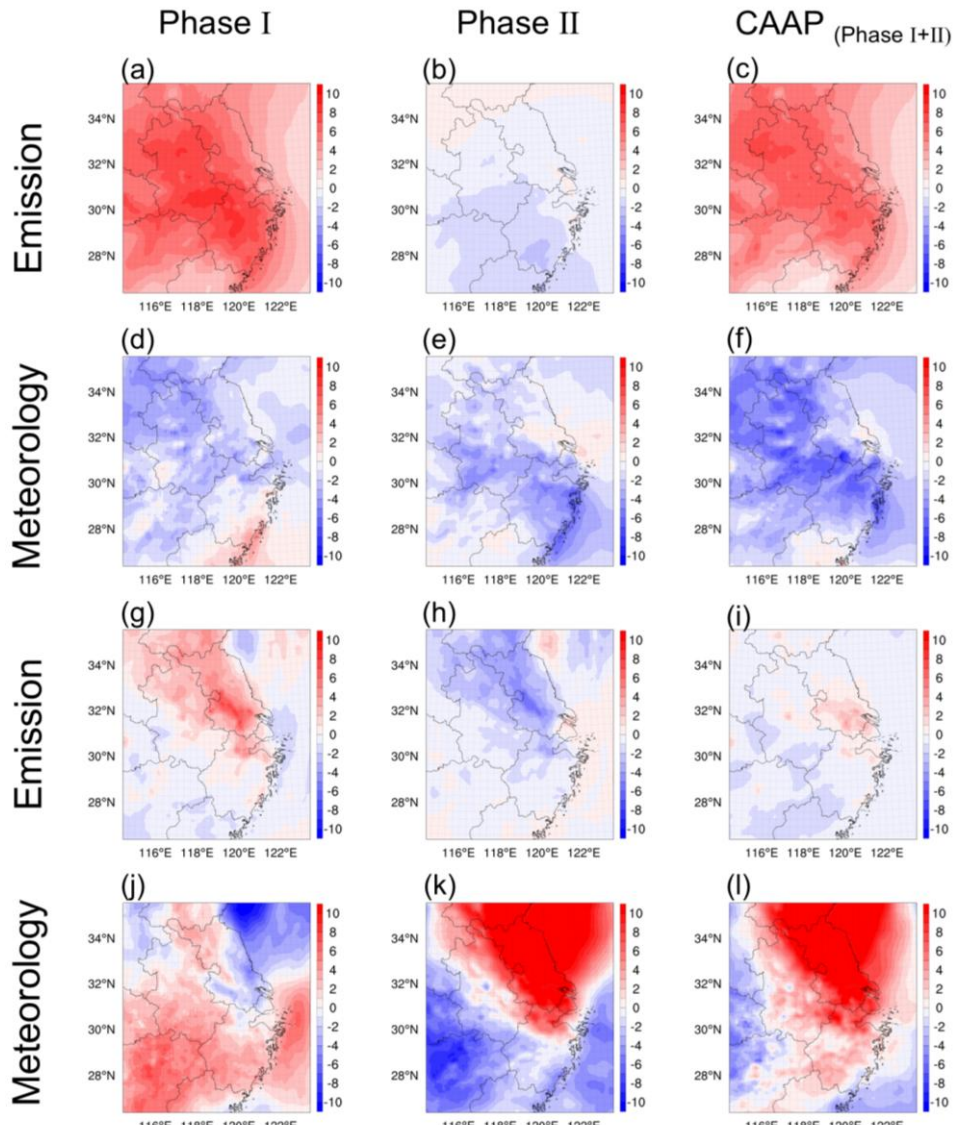
227 **3.1 Attribution of historical seasonal O₃ changes to emissions and meteorology**

228 A set of attribution simulations (SET1) with aerosol processes disabled (NOALL) and fixed 2020 meteorology was
229 conducted to isolate emission-driven O₃ variability in the YRD over the past decade, with the resulting responses shown in
230 Figure 3. During Phase I, emission reductions unexpectedly led to O₃ increases of 6.3 ppb in winter and 1.3 ppb in summer. In
231 contrast, Phase II witnessed coordinated NOx and VOCs controls, leading to O₃ reductions of 0.9 ppb (winter) and 1.5 ppb

(summer). These contrasting outcomes reflect the nonlinear chemistry of O₃ formation. While Phase I focused primarily on reducing PM_{2.5} and SO₂, VOCs emissions remained poorly regulated and even increased, enhancing photochemical activity. In contrast, Phase II adopted a more balanced control strategy targeting both NOx and VOCs, which proved more effective in mitigating O₃ pollution. Spatially, the strongest O₃ responses occurred in the northwestern and central parts of the YRD, aligning with regions that experienced the largest emission reductions.

To assess the influence of meteorological conditions, we fixed anthropogenic emissions at 2013 levels and varied the meteorological fields across years. Results revealed seasonally asymmetric impacts: meteorology contributed to wintertime O₃ declines (1.7 ppb and 2.1 ppb during Phases I and II, respectively), but promoted summertime O₃ increases (1.4 ppb and 4.6 ppb). This highlighted a distinct seasonal asymmetry in meteorological influences on O₃. As summarized in Table S3, changes in five key meteorological parameters (shortwave radiation (SW), temperature (T₂), relative humidity (RH₂), planetary boundary layer height (PBLH), and wind speed (WS₁₀)) collectively explain these trends. In winter, lower radiation and T₂, higher RH₂, and stronger WS₁₀ suppressed O₃ formation and accumulation. Conversely, summer conditions characterized by higher radiation and T₂, coupled with lower RH₂ and weaker WS₁₀, favored O₃ build-up. Although this study does not explicitly quantify the relative contributions of individual meteorological factors, prior studies (Liu et al., 2023a; Yan et al., 2024; Dai et al., 2024) using multiple linear regression consistently identify SW and T₂ as dominant drivers. Figure S4 presented the spatial distributions of meteorological changes during 2013-2020, revealing that the most pronounced shifts—especially in radiation and temperature—occurred in the central YRD and were more significant in summer, consistent with stronger O₃ responses.

In summary, anthropogenic emission changes were the dominant drivers of winter O₃ increases during Phase I. These findings are consistent with earlier research (Cao et al., 2022; Wu et al., 2022), which similarly highlighted that early-phase air quality interventions—though effective in reducing PM_{2.5}—often overlooked the complex chemistry of O₃, particularly the roles of VOCs and NOx, thereby unintentionally intensifying O₃ pollution. The transition to coordinated multi-pollutant control strategies in Phase II enabled more effective O₃ mitigation. In addition, the role of meteorology was non-negligible. Our findings, in line with those of Liu and Wang (2020), emphasize a pronounced seasonal asymmetry—meteorology suppressed winter O₃ but enhanced summer levels. Notably, wintertime O₃ variability was primarily emission-driven during Phase I, but increasingly influenced by meteorology in Phase II. In contrast, summer O₃ changes were consistently dominated by meteorological variability across both phases. These insights underscore the need for future O₃ control strategies to account for both emissions and meteorological variability, particularly in the context of climate change and evolving pollution regimes. These externally driven O₃ changes provide the foundation for evaluating how aerosol-mediated processes further modulate the emission-driven portion of the O₃ response.

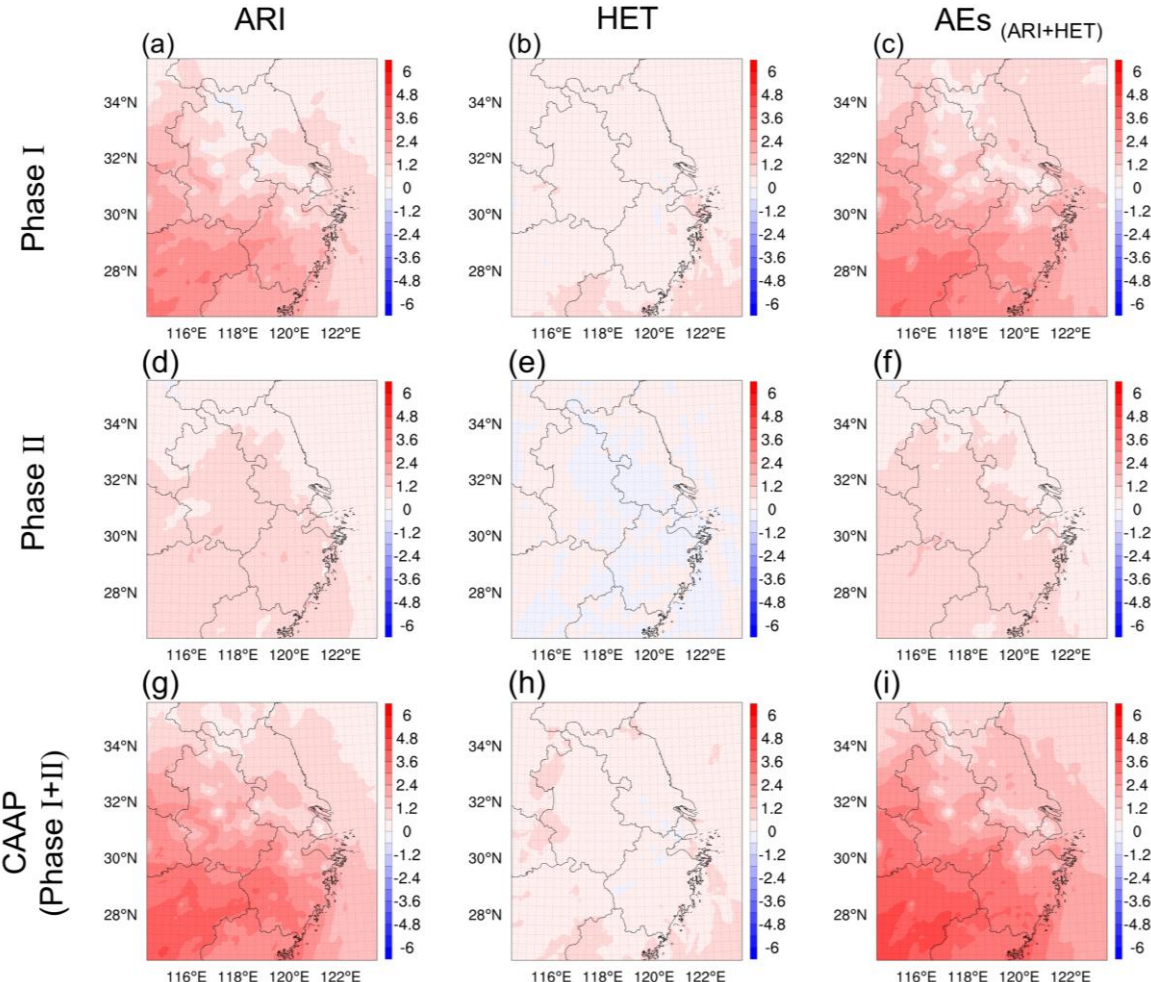


261
262 **Figure 3** Attribution of seasonal O₃ variations (ppb) in the Yangtze River Delta to emission reductions (a–c, g–i) and
263 meteorological influences (d–f, j–l) during Phase I and Phase II of the CAAP, with winter and summer results displayed in
264 the upper and lower rows, respectively.

265 **3.2 Aerosol multi-effects contributions to past seasonal O₃ variations**

266 Building on the external drivers identified in Section 3.1, we next examined how ARI and HET modified the emission-
267 reduction-driven O₃ response. Figure 4 illustrated the wintertime spatial patterns of O₃ changes driven by ARI and HET across
268 the YRD during both phases of the CAAP. In Phase I, ARI induced a significant O₃ increase of up to 1.14 ppb across the region,
269 while the contribution from HET was notably smaller at 0.32 ppb. This indicated that early aerosol reductions primarily
270 enhanced O₃ via increased solar radiation and associated meteorological feedbacks, rather than through the suppression of
271 radical uptake on particle surfaces. This finding contrasted with those of Li et al. (2019a), who—using GEOS-Chem
272 simulations—attributed O₃ increases over the BTH to reduced HO₂ uptake under declining PM_{2.5}. The discrepancy may stem
273 from differences in model representation; our framework explicitly incorporates both ARI-driven meteorological feedbacks
274 and the direct photolysis attenuation by aerosols, enabling a more comprehensive simulation of aerosol–radiation interaction.

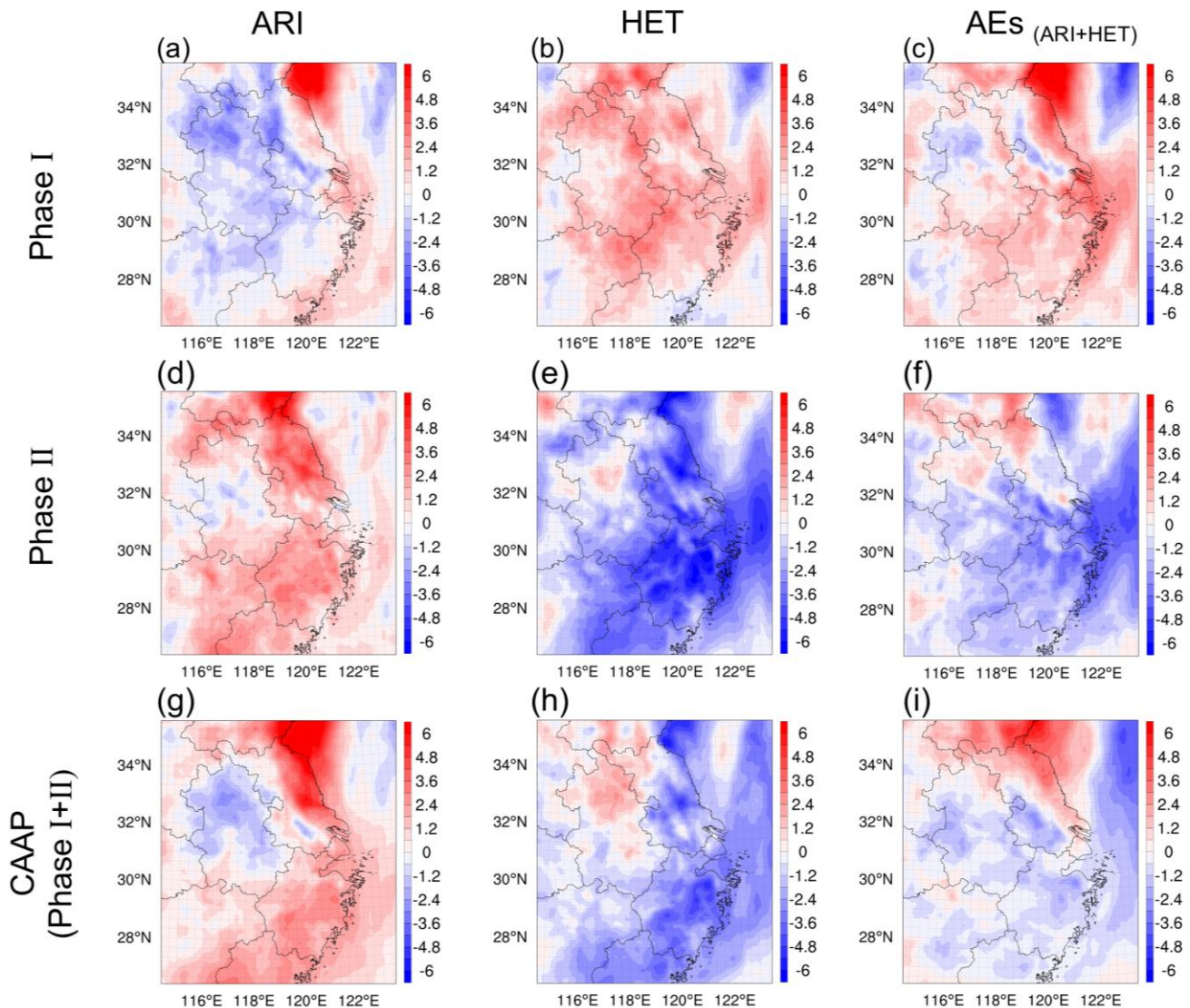
275 During Phase II, the ARI-induced O_3 increase weakened to +0.74 ppb, and the contribution from HET became negligible or
 276 slightly negative (-0.01 ppb). This suggested that ARI remained the dominant aerosol-related driver of winter O_3 variability,
 277 while the influence of HET diminished. The reduced overall aerosol impact during this phase was consistent with smaller
 278 primary $PM_{2.5}$ emission reductions (-8% in Phase II compared to -37% in Phase I). Summing the contributions from both
 279 mechanisms, the total aerosol-driven O_3 enhancement reached +1.46 ppb in Phase I and +0.73 ppb in Phase II, culminating in
 280 a net wintertime increase of +2.2 ppb over the CAAP period.



281
 282 **Figure 4** Spatial distribution of winter O_3 changes (ppb) over YRD driven by ARI (a, d, g), HET (b, e, h) and their combined
 283 effects (AEs, c, f, i) during two stages of the CAAP.

284 In contrast to winter, summertime O_3 responses to AEs revealed different dominant mechanisms and magnitudes, as
 285 shown in Figure 5. In Phase I, HET played a more substantial role, contributing a 1.62 ppb increase, whereas ARI slightly
 286 suppressed O_3 by 0.51 ppb. This pattern indicated that under high photochemical activity, reduced particulate matter
 287 significantly weakened radical scavenging, thereby elevating HO_2 levels and promoting O_3 formation. During Phase II,
 288 however, HET unexpectedly contributed a 2.86 ppb decreases in O_3 , while ARI induced a 1.56 ppb enhancement. The HET-
 289 driven decrease may be linked to complex nonlinear chemical responses under further reduced aerosol backgrounds, which
 290 diminished the amplification effect of radical availability. Across both phases, HET consistently emerged as the primary driver
 291 of summertime aerosol-related O_3 variability. When aggregated, aerosols contributed a 1.11 ppb increase in Phase I and a 1.30

292 ppb decrease in Phase II, yielding a modest net summer reduction of 0.19 ppb over the CAAP period.

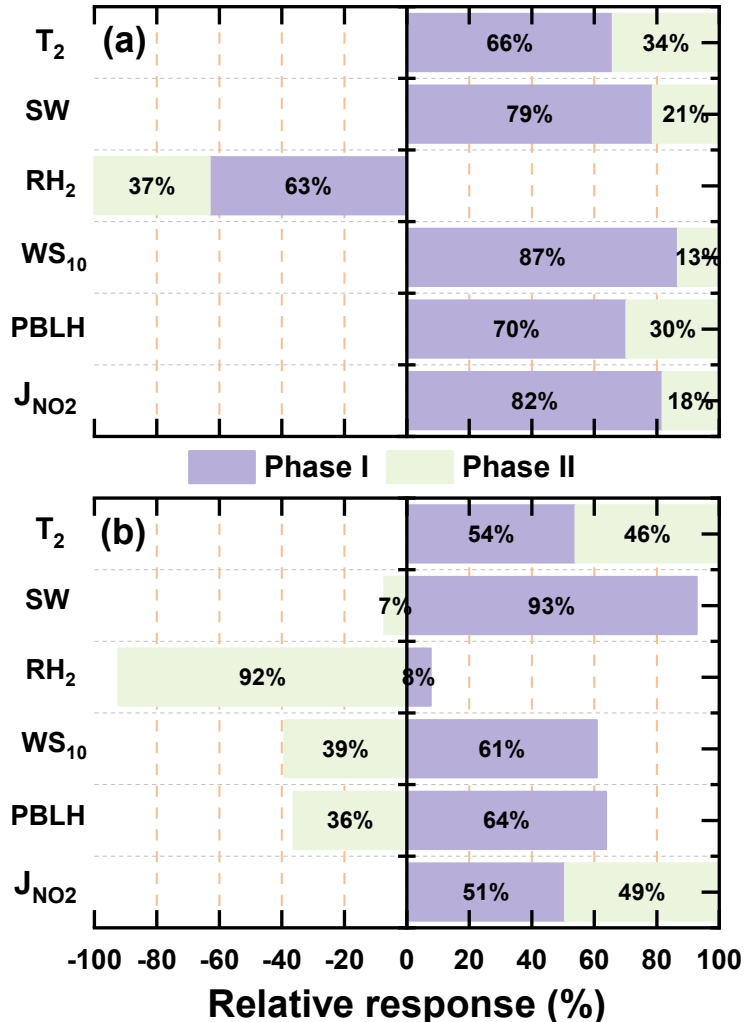


293

294 **Figure 5** Spatial distribution of summer O₃ changes (ppb) over YRD driven by ARI (a, d, g), HET (b, e, h) and their
295 combined effects (AEs, c, f, i) during two stages of the CAAP.

296 To elucidate the underlying mechanisms of aerosol impacts on O₃, we examined the changes in key meteorological
297 variables, photolysis rates, and HO₂ radical concentrations induced by ARI and HET during the two implementation phases of
298 the CAAP. Figure 6 presented the variations in five key meteorological parameters and the NO₂ photolysis rate (J_{NO₂}) in winter
299 and summer as influenced by ARI. The results indicated that ARI consistently enhanced J_{NO₂}, SW, T₂, WS₁₀, and PBLH, while
300 reducing RH₂ during winter across both phases. These modifications—especially increased SW and T₂—significantly
301 facilitated photochemical O₃ production, thereby elevating O₃. Notably, the magnitude of these changes was substantially
302 greater in Phase I than in Phase II, which can be attributed to the more pronounced reductions in aerosol emissions during the
303 earlier phase. In summer, ARI and HET exerted contrasting influences on ground-level O₃, with their effects reversing between
304 the two phases. ARI led to a slight decrease in O₃ (-0.51 ppb), likely due to enhanced vertical mixing from reduced aerosol
305 extinction, which increased solar radiation and photolysis rates. However, the concurrent rise in temperature and PBLH may

306 have diluted surface O_3 in certain regions (Figure 6b), resulting in a net negative O_3 response to ARI during this phase. In
 307 Phase II, the ARI-induced increases in T_2 and photolysis rates more effectively enhanced photochemical O_3 production.
 308 Simultaneously, reductions in PBLH and WS_{10} during this period suppressed vertical and horizontal O_3 dispersion (Figure 6b),
 309 collectively leading to a net positive O_3 response (+1.56 ppb).

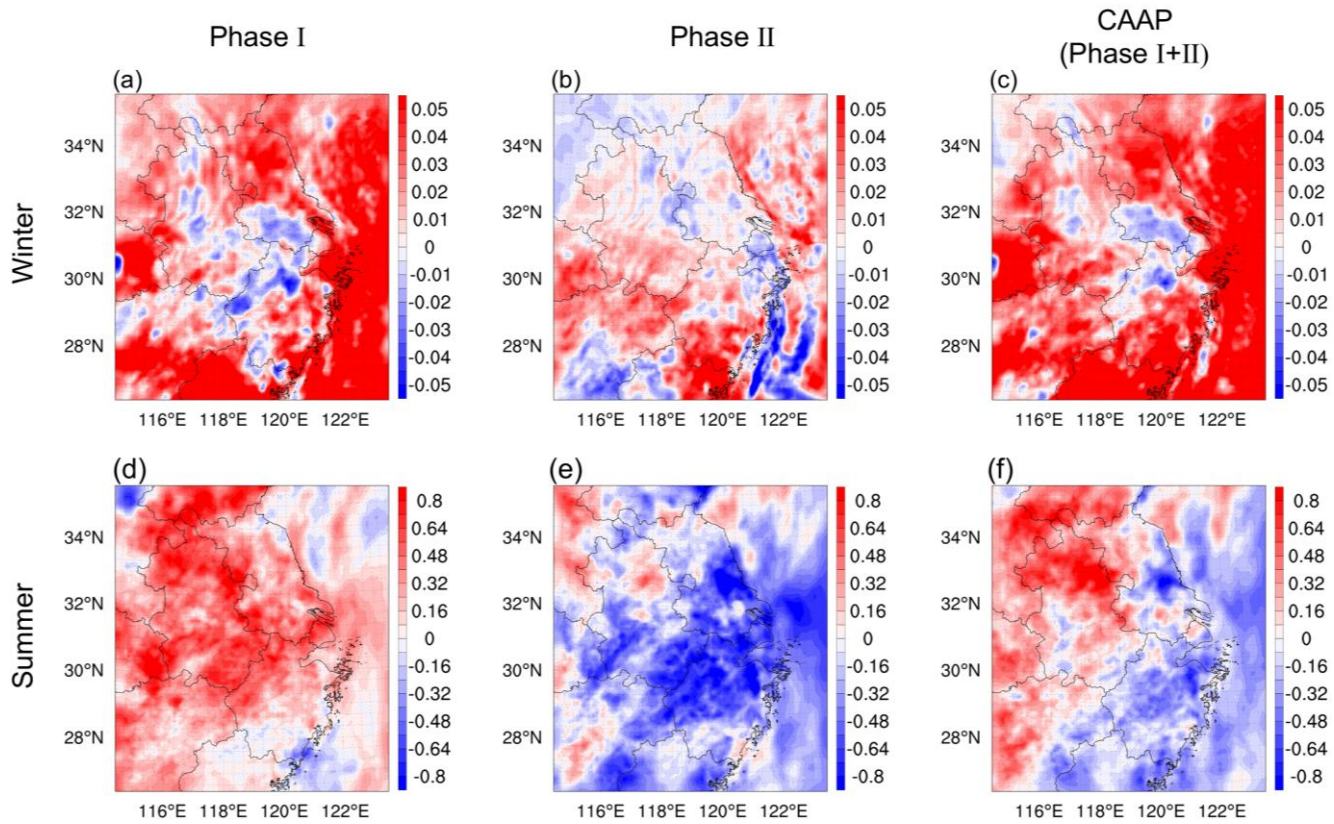


310

311 **Figure 6** ARI-driven relative responses of meteorological fields and photolysis rates in YRD during winter (a) and summer (b)
 312 for the two CAAP stages.

313 During Phase I, the substantial reductions in aerosol mass and surface area primarily weakened HO_2 heterogeneous uptake,
 314 as indicated by elevated HO_2 (Figure 7d). This reduction in radical loss increased the availability of HO_2 and OH, leading to
 315 an enhancement in the photochemical ozone production term $P(O_3)$ (Dyson et al., 2023). In parallel, N_2O_5 also increased during
 316 Phase I (Figure S5a), consistent with suppressed heterogeneous hydrolysis under reduced aerosol liquid water (ALW) and
 317 diminished aerosol surface area (Brown and Stutz, 2012). The weakened N_2O_5 hydrolysis further limited nighttime conversion
 318 of reactive nitrogen to HNO_3 , maintaining NO_x in more photochemically active forms (Ma et al., 2023b). Meanwhile,
 319 heterogeneous NO_2 uptake—an important $HONO$ source—was significantly reduced, consistent with the simulated decrease
 320 in $HONO$ (Figure S5d). The reduction in $HONO$ slightly weakened early-morning radical initiation (Yu et al., 2022), but this
 321 influence was outweighed by the strong enhancement in HO_2 and the limited conversion of NO_x into HNO_3 . As a result, HET

322 exerted a net positive contribution to O₃ (+1.62 ppb) in Phase I. In contrast, Phase II exhibited a fundamentally different
323 chemical response. Although aerosol loadings continued to decrease, the relative importance of heterogeneous pathways
324 shifted substantially. HO₂ declined during Phase II (Figure 7e), indicating a reduced radical pool and weaker propagation of
325 daytime photochemical production. At the same time, N₂O₅ decreased markedly (Figure S5b), suggesting that nighttime
326 NO₃/N₂O₅ chemistry became less effective at sustaining reactive nitrogen cycling under even lower aerosol surface area and
327 ALW. Rather than promoting efficient nighttime NO_x recycling, this suppression favored a net loss of reactive nitrogen through
328 terminal sinks (e.g., HNO₃), shifting NO_x partitioning toward less photochemically active forms and weakening daytime P(O₃).
329 Conversely, HONO concentrations rebounded during Phase II (Figure S5e). This increase reflects the altered balance between
330 NO₂ uptake and nighttime NO_x partitioning under reduced N₂O₅ hydrolysis. However, despite this HONO increase, its positive
331 effect on radical initiation could not compensate for the combined decline in HO₂, weakened N₂O₅ hydrolysis, and enhanced
332 HNO₃ formation (George et al., 2015). The joint effect was a net reduction in the morning radical pool and diminished
333 photochemical O₃ production (-2.86 ppb). This multi-pathway adjustment explains the observed sign reversal of HET's effect
334 on O₃ between the two phases and underscores the importance of considering the full suite of heterogeneous processes—rather
335 than radical uptake alone—when interpreting aerosol-mediated O₃ responses. In future work, we plan to apply integrated
336 process rate (IPR) diagnostics to more directly evaluate how individual heterogeneous pathways—such as HO₂ uptake, HONO
337 formation, and N₂O₅ hydrolysis—shape the resulting O₃ responses. Coupled with continued improvements in heterogeneous
338 chemistry parameterizations and more comprehensive constraints on radical, reactive nitrogen, and aerosol liquid water fields,
339 this will enable a more detailed and process-resolved understanding of phase-dependent O₃ changes.



340
341 **Figure 7** Spatial distributions of HO₂ concentration (ppt) changes induced by HET in winter (a-c) and summer (d-f) during
342 two phases of the CAAP in YRD.

343 To further evaluate whether daytime and nighttime O₃ responses compensate within the daily mean metric, we examined
344 the diurnal cycles of baseline O₃ concentration and the aerosol-mediated impacts (HET, ARI, and AEs) during Phase I, Phase
345 II, and the overall CAAP period for both winter (Figure S6) and summer (Figure S7). Across all phases and both seasons, the
346 dominant O₃ perturbations occur during daytime hours, coinciding with the photochemical peak at 14–16 LT. In winter, Phase
347 I exhibits a pronounced daytime enhancement driven by ARI (up to ~2.41 ppb), whereas HET induces a consistently positive
348 but comparatively weaker increase (up to ~0.49 ppb). In Phase II, the ARI-induced enhancement weakens notably (peaking at
349 ~1.24 ppb), and HET-induced changes remain minor. In summer, the diurnal behavior more clearly reflects a daytime -
350 dominated response. During Phase I, HET produces a marked midday O₃ enhancement (up to ~2.01 ppb), while ARI imposes
351 a weaker yet persistent negative contribution. In contrast, Phase II is characterized by a strong HET-driven daytime O₃ decrease
352 (maximum ~3.43 ppb), overwhelming the comparatively modest positive ARI effect. For all cases, nighttime O₃ changes share
353 the same direction as daytime responses but remain substantially smaller in magnitude, insufficient to offset the daytime signals
354 dominated by photochemistry. These diurnal patterns confirm that the phase-dependent O₃ responses to aerosol effects are not
355 artifacts of day–night compensation in daily mean metrics, but instead arise from robust, daytime-dominant photochemical
356 adjustments.

357 Previous studies showed that ARI and HET were not fully independent and could interact through aerosol–meteorology–
358 chemistry feedbacks (Chen et al., 2019; Liu et al., 2023b; Kong et al., 2018; Li et al., 2020a). ARI-induced increases in near-
359 surface relative humidity typically enhanced aerosol hygroscopic growth and expanded aerosol surface area. The resulting

360 increase in aerosol liquid water promoted gas-to-particle partitioning and facilitated aqueous- and surface-phase reactions,
361 thereby accelerating heterogeneous oxidation pathways involving SO_2 and NO_x . The strengthened heterogeneous formation
362 of secondary inorganic aerosols further modified solar radiation and potentially intensified the ARI effect. In the present study,
363 our primary focus was to quantify the separate and combined contributions of ARI and HET to O_3 changes across different
364 stages of the CAAP. Accordingly, we isolated their individual impacts rather than examining their nonlinear coupling. We
365 acknowledged that ARI–HET interactions might also affect O_3 under certain chemical and meteorological conditions, and we
366 indicated that future work would incorporate dedicated coupled-sensitivity experiments to more explicitly quantify these
367 nonlinearities and their implications for O_3 formation.

368 Figure S8 illustrated the hierarchical relationships among the four factors analyzed in this section. Emission reductions
369 and meteorological variability constituted the external drivers of O_3 changes, whereas ARI and HET acted as aerosol-mediated
370 modulators that adjust the emission-reduction-driven O_3 responses. This framework motivated our presentation sequence,
371 where external drivers were examined first, followed by the modulation effects of ARI and HET. Figure 8 presented the relative
372 contributions of major driving factors to surface O_3 changes during the two phases of the CAAP. In winter, anthropogenic
373 emissions emerged as the dominant driver of O_3 increases during Phase I, contributing 6.3 ppb, primarily due to enhanced
374 photochemical production under VOCs-limited conditions. In contrast, Phase II saw a modest O_3 decline (0.9 ppb) resulting
375 from co-reductions in NO_x and VOCs, suggesting improved control effectiveness through coordinated precursor mitigation.
376 Meteorological changes consistently exerted a suppressive effect on wintertime O_3 , contributing -1.7 ppb and -2.1 ppb in
377 Phases I and II, respectively. AEs—mediated by ARI and HET—also contributed to O_3 accumulation, particularly in Phase I
378 ($+1.46$ ppb), though their influence weakened in Phase II ($+0.73$ ppb) due to the smaller reductions in aerosol loading. Overall,
379 the wintertime O_3 increase in Phase I was jointly driven by emissions and aerosol-related processes, while the slight decline
380 in Phase II reflected the synergistic benefits of emission reductions and favorable meteorological conditions. In contrast, the
381 attribution profile for summer revealed a dominant role of meteorology. Meteorological variability accounted for a substantial
382 O_3 increase in Phase II ($+4.6$ ppb), outweighing the contributions of emission changes. The effect of emission reductions on
383 summer O_3 was limited and nonlinear: a slight increase ($+1.3$ ppb) was observed in Phase I, followed by a minor decline (-1.5
384 ppb) in Phase II, indicative of a photochemical regime with weak emission sensitivity. Aerosol-related effects exhibited strong
385 seasonal contrasts. HET was the dominant mechanism influencing O_3 in both summer phases, albeit with opposite signs—
386 enhancing O_3 by 1.62 ppb in Phase I but reducing it by 2.86 ppb in Phase II. These contrasting effects likely reflect differences
387 in HO_2 uptake efficiency under evolving humidity and temperature conditions. ARI effects were comparatively modest, leading
388 to a slight O_3 decrease in Phase I (0.51 ppb) and an increase in Phase II (1.56 ppb), likely driven by enhanced photolysis and
389 reduced vertical mixing.

390 Collectively, these results highlight the evolving interplay among emission control efforts, meteorological conditions, and

aerosol effects in shaping surface O_3 trends. While anthropogenic emissions primarily drove winter O_3 increases during the early phase of the CAAP, the roles of meteorology and aerosol processes became increasingly prominent in summer and in the later policy phase. This multi-factor attribution framework aligns well with prior modeling and observational studies in eastern China (Zhu et al., 2021; Zhou et al., 2019). For example, Liu et al. (2023a) demonstrated that declining $PM_{2.5}$ levels enhanced O_3 formation by weakening HO_2 radical scavenging, particularly under VOCs-limited regimes—a conclusion consistent with our wintertime results. Similarly, Yang et al. (2019) highlighted the growing influence of meteorological variability in recent years as the sensitivity of O_3 to emission changes has diminished. Our study extends this knowledge base by providing phase-resolved attribution and explicitly separating the effects of ARI and HET. Notably, the reversal of HET-driven O_3 responses in summer—from enhancement to suppression—has rarely been quantified and underscores the importance of dynamically characterizing aerosol–ozone interactions under evolving atmospheric and policy contexts.

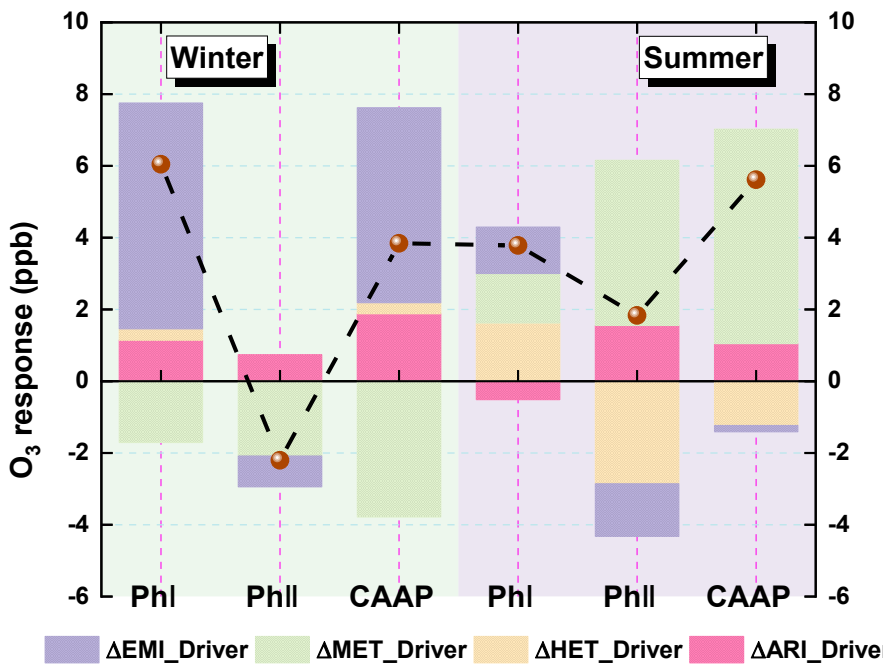
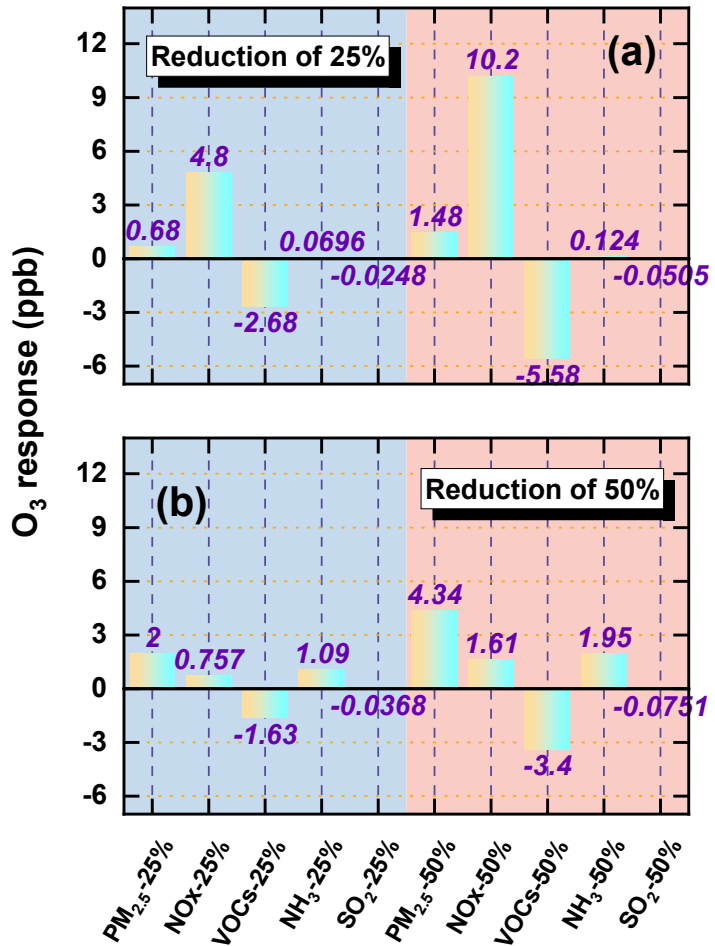


Figure 8 Quantitative attribution of surface O_3 changes over the Yangtze River Delta (YRD) during the two CAAP phases. Contributions from emission reductions (EMI), meteorological variability (MET), aerosol–radiation interactions (ARI), and heterogeneous chemistry (HET) are shown for winter (left) and summer (right).

3.3 O_3 responses to precursor emission reductions under aerosol effects

Before presenting the simulation results, we first assessed the O_3 chemical regimes over YRD using the widely adopted H_2O_2/HNO_3 ratio (Jeon et al., 2018; Peng et al., 2011; Hammer et al., 2002; Zhang et al., 2000). This metric serves as a diagnostic indicator of O_3 production sensitivity, with ratios <0.6 indicating VOCs-limited conditions, >0.8 denoting NOx-limited regimes, and intermediate values representing transitional states. Figure S9 showed the spatial distribution of this ratio under the baseline scenario (20E20M_AEs). The analysis reveals that wintertime O_3 formation is predominantly VOCs-limited across the YRD, while in summer, most areas exhibit transitional or NOx-limited regimes, except parts of Anhui Province. Figure 9 displayed the simulated O_3 responses to precursor reductions in both seasons. The results highlight strong seasonal

413 differences and nonlinear sensitivities depending on chemical regime. In winter, reductions in primary PM_{2.5} and NOx led to
414 substantial O₃ increases. Specifically, 25% and 50% reductions in PM_{2.5} increased O₃ by 0.7 ppb and 1.5 ppb, respectively,
415 while NOx reductions caused even larger enhancements of 4.8 ppb and 10.2 ppb. These increases primarily stem from
416 weakened aerosol suppression mechanisms—namely reduced heterogeneous uptake and increased photolysis rates—which
417 enhance radical availability and photochemical activity. Additionally, under VOCs-limited conditions, NOx reductions
418 diminish O₃ titration by NO, further contributing to O₃ accumulation. Among all precursors, NOx reductions produced the
419 most pronounced O₃ increase. In contrast, NH₃ and SO₂ reductions exerted negligible impacts on O₃, underscoring their limited
420 roles in direct O₃ photochemistry. VOCs controls, on the other hand, effectively suppressed O₃ formation, with 25% and 50%
421 reductions yielding decreases of 2.7 ppb and 5.6 ppb, respectively. In summer, O₃ responses followed broadly similar trends
422 but with different magnitudes. Reducing PM_{2.5} and NOx increased O₃ by 2 ppb and 4.3 ppb (PM_{2.5}) and 0.8 ppb and 1.6 ppb
423 (NOx), respectively. Notably, the O₃ increase associated with PM_{2.5} reductions exceeded that from NOx cuts, underscoring the
424 critical role of particulate matter in regulating radical chemistry via aerosol-mediated pathways. VOCs reductions remained
425 the only control strategy that consistently decreased O₃, lowering concentrations by 1.6 ppb and 3.4 ppb for 25% and 50%
426 reductions, respectively. Again, NH₃ and SO₂ reductions had negligible effects. Collectively, these findings suggest that
427 continued PM_{2.5}-targeted controls may inadvertently worsen O₃ pollution under active AEs, particularly in summer. In contrast,
428 VOCs mitigation remains the most robust and seasonally effective strategy for O₃ reduction.



429

430 **Figure 9** O₃ concentration changes (ppb) in response to 25% and 50% reductions in precursor emissions over YRD during
431 winter (a) and summer (b).

432 Figure S10 presented the distribution of O₃ changes under 25% and 50% precursor reductions for both seasons. Strong
433 seasonal contrasts and regional gradients in O₃ responses are evident. Reductions in PM_{2.5} consistently caused widespread O₃
434 increases across the YRD, with the most pronounced enhancements in northwestern inland regions—particularly southern
435 Jiangsu and central-to-northern Anhui—where historically high aerosol burdens make O₃ formation especially sensitive to
436 weakened aerosol suppression (via ARI and HET). Conversely, coastal cities such as Shanghai and eastern Zhejiang exhibited
437 smaller O₃ increases, reflecting their lower baseline aerosol concentrations and weaker aerosol feedbacks. VOCs reductions
438 led to the largest O₃ decreases in urban corridors, particularly along the Shanghai–Nanjing–Hangzhou (SNH) axis, where
439 VOCs emissions are elevated and O₃ formation is strongly VOCs-sensitive. NOx reductions yielded seasonally opposite effects:
440 in winter, O₃ increased broadly across the YRD, while in summer, decreases were observed in most regions except Anhui
441 Province. These patterns align with seasonal chemical regimes inferred from H₂O₂/HNO₃ ratios—VOCs-limited in winter and
442 NOx-limited or transitional in summer. NH₃ and SO₂ reductions produced negligible spatial effects in both seasons, reinforcing
443 their limited involvement in direct O₃ photochemistry. These spatially heterogeneous responses highlight the need for
444 geographically differentiated control strategies. Regions with historically high aerosol pollution are more likely to experience
445 unintended O₃ increases following PM_{2.5} or NOx reductions. Conversely, VOCs control provides consistent and widespread

446 O_3 benefits across both seasons, making it a key lever for achieving co-benefits in both $PM_{2.5}$ and O_3 mitigation.

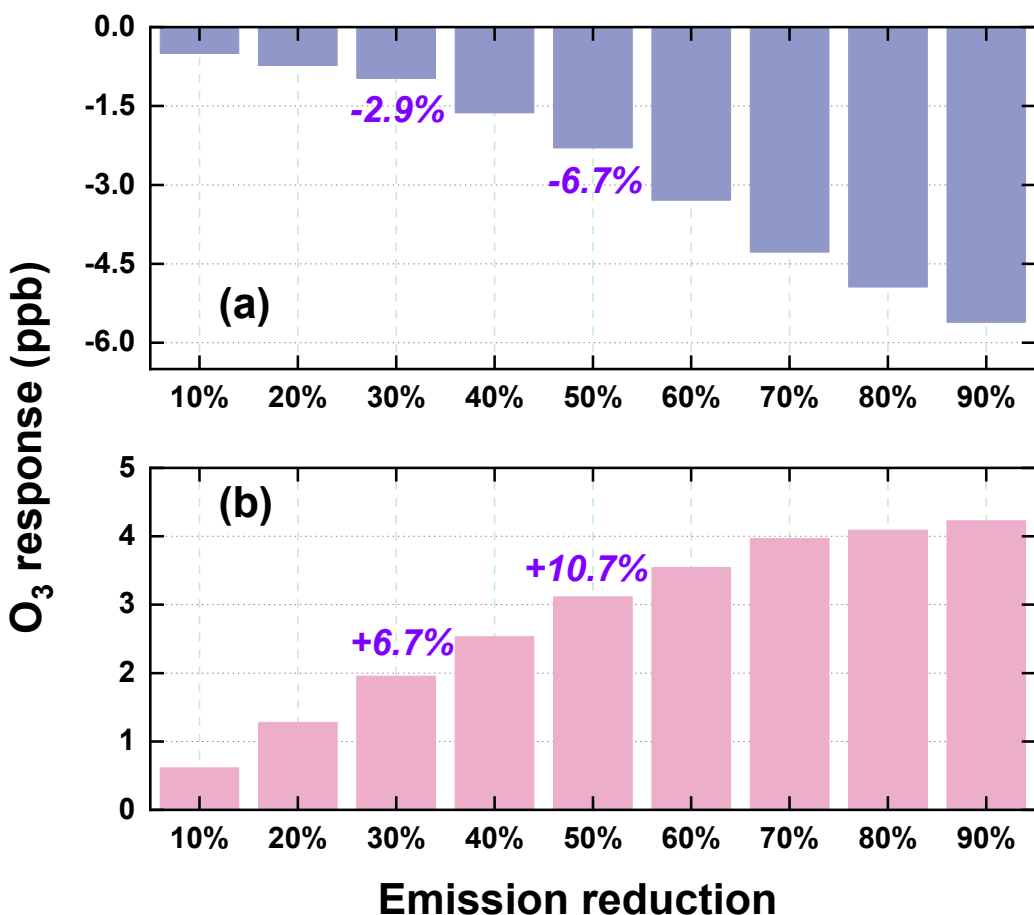
447 To better understand the temporal dynamics of O_3 responses, we analyzed diurnal variations in four representative cities—
448 Shanghai, Nanjing, Hangzhou, and Hefei—under 50% reductions of individual precursors (Figure S11). In winter, NOx
449 reductions led to substantial O_3 increases during afternoon hours (14:00–17:00), particularly in urban centers like Shanghai
450 and Hangzhou, where enhancements exceeded 15 ppb. These increases reflect the dual effect of diminished NO titration and
451 enhanced photochemical activity. $PM_{2.5}$ reductions also caused moderate O_3 increases from late morning to early afternoon,
452 underscoring the influence of both ARI and HET. VOCs reductions induced midday O_3 declines (12:00–15:00) exceeding 5
453 ppb, consistent with VOCs-limited wintertime chemistry. In summer (Figure S12), VOCs reductions suppressed O_3 throughout
454 the daytime, with maximum declines reaching up to 25 ppb in early afternoon, reaffirming the effectiveness of VOCs control.
455 In contrast, $PM_{2.5}$ reductions led to notable O_3 increases during photochemically active hours (11:00–16:00), highlighting the
456 critical role of aerosols in modulating radical cycles and O_3 production. Overall, these diurnal profiles underscore the time-
457 sensitive nature of O_3 responses to precursor emission reductions. They emphasize the necessity for temporally and spatially
458 refined control strategies that account for local photochemical regimes, emission structures, and AEs.

459 **3.4 Future O_3 responses to Carbon neutrality–driven emission reductions considering aerosol effects**

460 We performed a suite of sensitivity experiments using the 2020 anthropogenic emissions as the baseline to examine
461 prospective O_3 responses to emission mitigation under China's carbon peaking and carbon neutrality pathways. As shown in
462 Figure 10, O_3 exhibited pronounced seasonal variability in response to progressive emission reductions. In winter, regional
463 mean O_3 increased monotonically with the magnitude of emission cuts, rising from +2.1% under the 10% reduction scenario
464 to +14.6% under the 90% scenario. This counterintuitive increase is primarily attributed to two synergistic mechanisms: (1)
465 reduced O_3 titration resulting from NOx emission reductions, and (2) weakened aerosol-mediated O_3 suppression due to lower
466 aerosol loads, which diminish both ARI and HET processes. The reduced availability of aerosol surfaces and optical attenuation
467 enhances photolysis rates and radical propagation, thereby promoting O_3 accumulation. In contrast, summer O_3 declined
468 steadily with increasing emission reductions, from -1.5% to -16.5% across the same range. This decline reflects the dominance
469 of VOCs-limited or transitional photochemical regimes in the region during summer, where coordinated reductions in NOx
470 and VOCs effectively suppress O_3 formation. These results underscore the seasonal asymmetry of O_3 responses under the
471 carbon-neutrality-aligned emission trajectories used in this study—namely the proportional precursor-reduction pathways
472 designed to reflect long-term, economy-wide emission declines. While such stringent reductions may inadvertently aggravate
473 wintertime O_3 pollution, they yield substantial co-benefits for summer O_3 mitigation. The spatial distribution of O_3 changes
474 under these scenarios, presented in Figure S13, further corroborates the contrasting seasonal patterns. In winter, O_3 increases
475 were most pronounced in inland areas of northern Anhui and central Jiangsu—regions characterized by historically high
476 aerosol burdens and stronger aerosol-mediated O_3 suppression. As emissions decline, the weakening of both aerosol effects

477 and NO_x titration leads to a disproportionate O₃ rebound in these locations. The largest summer O₃ reductions observed in
 478 densely populated urban corridors such as Shanghai, Nanjing, and Hangzhou. These metropolitan areas, with high precursor
 479 emissions and transitional or NO_x-limited chemical regimes, are particularly responsive to coordinated VOCs and NO_x
 480 controls. The spatial heterogeneity in O₃ responses highlights the necessity of designing region-specific and seasonally
 481 adaptive emission control strategies. Differentiated approaches are essential given the diverse pollution histories, chemical
 482 sensitivities, and aerosol–ozone coupling characteristics across the YRD.

483 Overall, these findings suggest that carbon neutrality–driven emission pathways, if carefully managed, can yield
 484 significant summertime O₃ mitigation benefits, but must be complemented with targeted wintertime strategies to avoid adverse
 485 trade-offs. The proportional 10–90% reductions applied uniformly across all pollutant species were designed as an idealized
 486 framework to systematically examine nonlinear O₃ responses under consistent boundary conditions. In practice, however,
 487 future emission pathways are expected to exhibit pronounced sectoral and spatial heterogeneity—for example, SO₂ and
 488 primary PM_{2.5} typically decline faster than VOCs and NH₃, and the pace of reductions varies across industrial, transportation,
 489 and residential sectors. Such differences may influence the magnitude of O₃ responses and the balance among precursor
 490 contributions. Recognizing this limitation, future work will incorporate sector-resolved and scenario-specific emission
 491 pathways to provide a more realistic assessment of O₃ sensitivity under evolving emission structures.



492
 493 **Figure 10** Seasonal variations in O₃ concentrations (ppb) projected under a range of emission reduction intensities (10%–90%),
 494 including representative scenarios for carbon peaking (30%) and carbon neutrality (50%), referenced to 2020 conditions with
 495 aerosol-related processes accounted for. Results for summer and winter are displayed in the upper and lower panels,

496 respectively.

497 3.5 Discussion and policy implications

498 This study presented a comprehensive assessment of O₃ responses to emission reductions under both the CAAP and future
499 carbon neutrality pathways, explicitly considering aerosol effects. Our findings underscore that while emission control
500 measures have been effective in substantially lowering PM_{2.5}, they may yield unintended consequences for O₃ pollution—
501 particularly under VOCs-limited regimes during winter. Specifically, aerosol-induced enhancements in O₃—via weakened
502 heterogeneous chemistry (HET) and increased photolysis (ARI)—highlight the necessity of accounting for multiphase
503 feedback mechanisms in the design of future air quality strategies. Our phase-resolved, seasonally differentiated attribution
504 analysis suggests that coordinated reductions in VOCs and NO_x are critical for effective O₃ mitigation, especially in summer
505 when photochemical activity is most intense. Furthermore, the spatial heterogeneity of O₃ responses calls for region-specific
506 strategies. For instance, in inland areas with historically high aerosol burdens, the potential for O₃ rebound due to weakened
507 aerosol suppression is more pronounced, necessitating tailored mitigation approaches. In contrast, urban corridors such as the
508 Shanghai–Nanjing–Hangzhou (SNH) axis—characterized by high VOCs emissions and transitional or NO_x-limited regimes—
509 stand to benefit most from targeted VOCs controls, particularly under future carbon-neutrality-driven reductions.

510 Uncertainties in HET parameterizations also introduce potential variability into the estimated O₃ responses. The uptake
511 coefficients (γ) for HO₂, NO₂, and N₂O₅ depend on aerosol liquid water content, acidity, ionic strength, and particle composition
512 (Jacob, 2000), yet these dependencies remain imperfectly constrained in current atmospheric models. As a result, uncertainties
513 in these parameters may alter the magnitude of individual heterogeneous pathways simulated in this study. For example, higher
514 assumed HO₂ uptake would strengthen radical loss and could reduce the positive HET contribution during Phase I, whereas
515 larger N₂O₅ hydrolysis rates would enhance nighttime conversion of NO_x to HNO₃ and potentially intensify the negative HET
516 influence in Phase II. Likewise, uncertainties in NO₂ uptake and HONO yields could modulate early-morning radical initiation
517 and shift the balance between radical propagation and reactive nitrogen recycling. Importantly, while such uncertainties may
518 influence the absolute magnitude of HET-induced O₃ perturbations, they are unlikely to overturn the direction of the response.
519 Prior modeling studies provide support for this robustness. For instance, Shao et al. (2021) showed that varying γ_{HO_2} between
520 0.2 and 0.08 altered the magnitude of the O₃ increase driven by reduced HO₂ heterogeneous uptake—from approximately 6%
521 (consistent with the ~7% reported by Li et al. (2019a) to about 2.5% during 2013–2016—yet the effect remained positive in
522 all cases. These findings indicate that although heterogeneous uptake assumptions can change the amplitude of the response,
523 the sign of the O₃ change is preserved because the underlying chemical mechanism (reduced radical loss leading to enhanced
524 photochemical production) remains the same. By analogy, the phase-dependent sign reversal identified in our study reflects a
525 structural shift in the competition among HO₂ uptake, N₂O₅ hydrolysis, and HONO formation pathways, and is therefore
526 unlikely to be reversed by plausible uncertainties in individual uptake coefficients. Our future studies will incorporate dedicated
527 sensitivity simulations and integrated process rate (IPR) diagnostics to more systematically quantify how uncertainties in

528 heterogeneous chemistry parameterizations propagate into O_3 simulations. Improvements in observational constraints on
529 aerosol acidity, liquid water content, and heterogeneous reaction rates will further strengthen mechanistic understanding and
530 reduce uncertainty in model-based assessments of aerosol– O_3 interactions under evolving emission pathways.

531 It is worth emphasizing that all simulations were performed under a fixed-meteorology configuration, which was designed
532 to isolate the influences of aerosol processes and emission changes on O_3 by suppressing interannual meteorological variability.
533 This strategy improves the interpretability of attribution results by reducing confounding weather effects, but it inevitably
534 constrains the model's ability to capture O_3 variability associated with meteorological extremes, such as heat waves or
535 anomalous circulation patterns. As a result, caution is warranted when extending these findings to long-term evolutions or
536 climate-change contexts, where interactions between emissions and meteorology may substantially alter O_3 responses. Future
537 work will explicitly address this limitation by conducting additional sensitivity experiments with time-varying meteorological
538 conditions.

539 These findings carry timely relevance for China's national climate and environmental goals. As outlined in the 14th Five-
540 Year Plan for Ecological and Environmental Protection and the 2060 Carbon Neutrality Roadmap, deep multi-sector emission
541 cuts are pivotal for achieving synergistic benefits between air quality improvement and climate change mitigation. Our results
542 demonstrate that under prevailing atmospheric chemical regimes—especially during winter—aggressive reductions in primary
543 $PM_{2.5}$ and NO_x may inadvertently exacerbate O_3 pollution unless accompanied by VOCs-focused controls and regionally
544 tailored strategies. In light of these findings, we advocate for an integrated policy framework that (i) coordinates VOCs and
545 NO_x reductions according to regional O_3 sensitivity, (ii) strengthens VOCs monitoring and inventory resolution at the city
546 level, and (iii) explicitly incorporates aerosol effects in both short-term air pollution forecasting and long-term carbon-
547 neutrality scenarios. Such targeted and mechanism-informed strategies will help bridge the current policy gap between $PM_{2.5}$
548 control and O_3 pollution mitigation, while ensuring co-benefits under evolving climate objectives.

549 **4. Conclusions**

550 We employed a phase- and season-specific WRF-Chem framework that explicitly accounted for aerosol–radiation
551 interactions and heterogeneous chemistry to characterize aerosol-driven modulation of O_3 over the YRD from 2013 to 2024.
552 Through combined analyses of emission transitions, meteorological variability, and carbon-neutrality-oriented scenarios, this
553 study provides an integrated assessment of the mechanisms governing historical O_3 changes and future responses to precursor
554 emission controls.

555 O_3 exhibited a distinct rise–fall trajectory over the past decade, shaped by complex interactions among emission
556 reductions, meteorological changes, and aerosol effects. During Phase I, substantial reductions in $PM_{2.5}$ and SO_2 , coupled with
557 inadequate VOCs controls, led to significant wintertime O_3 increases (6.29 ppb) and modest summer increases (1.28 ppb). In

558 Phase II, more balanced reductions in NO_x and VOCs effectively suppressed O₃ formation. Meteorological variability also
559 exhibited seasonally asymmetric impacts—suppressing O₃ in winter but enhancing accumulation in summer. While wintertime
560 O₃ changes were primarily driven by emissions, summertime variations were dominated by meteorological factors. Aerosol
561 effects further modulated O₃ concentrations through seasonally distinct mechanisms. In winter, ARI played the dominant role:
562 the substantial aerosol reductions in Phase I enhanced solar radiation and boundary layer development, promoting O₃ formation
563 (1.14 ppb); these effects weakened in Phase II (0.73 ppb). Summer O₃ was more sensitive to HET. In Phase I, aerosol
564 decreases weakened heterogeneous radical uptake, enhancing O₃ formation (+1.62 ppb). In Phase II, however, the net HET
565 effect reversed sign (-2.86 ppb), driven by shifts in multiple heterogeneous pathways—including changes in radical uptake,
566 HONO and N₂O₅ chemistry, and aerosol liquid water—rather than radical scavenging alone.

567 Accounting for aerosol effects, precursor emission reductions elicited marked seasonal and spatial O₃ responses. In winter,
568 a 50% reduction in VOCs effectively suppressed O₃ by 5.58 ppb, whereas equivalent reductions in NO_x and PM_{2.5} increased
569 O₃ by 10.2 ppb and 1.48 ppb, respectively—primarily due to weakened O₃ titration and radical loss processes. In summer,
570 reductions in PM_{2.5} led to greater increases in O₃ than NO_x (4.34 ppb vs. 1.61 ppb under the 50% reduction scenario),
571 highlighting the crucial role of aerosol effects in shaping photochemical O₃ production. Under carbon neutrality–driven
572 emission reduction scenarios, O₃ exhibited pronounced seasonally contrasting responses. In winter, O₃ increased
573 monotonically with the magnitude of emission cuts, primarily due to the weakened titration by NO and the diminished aerosol-
574 mediated suppression via heterogeneous chemistry and radiation attenuation. In contrast, summer O₃ consistently declined,
575 with the most substantial improvements observed in high-emission urban corridors. These reductions were mainly driven by
576 the synergistic control of NO_x and VOCs under NO_x-limited and transitional photochemical regimes. When aerosol effects
577 were considered, wintertime O₃ increased by 6.7% and 10.7% under carbon peaking and neutrality scenarios, respectively,
578 whereas summertime O₃ decreased by 2.9% and 6.7%, highlighting the critical role of multiphase aerosol effects in shaping
579 future air quality outcomes and making climate mitigation strategies.

580 While this study provides innovative and policy-informative findings, several uncertainties remain that warrant further
581 investigation. Uncertainties primarily arise from limitations in the parameterization of heterogeneous chemistry, assumptions
582 in future emission projections, and the current resolution of VOCs emission inventories. Future efforts should prioritize the
583 enhancement of real-time VOCs monitoring, vertical profiling of O₃ and its precursors, and the refinement of multiphase
584 chemical processes in regional models. In conclusion, a holistic and mechanism-informed approach—one that jointly accounts
585 for emissions, aerosol effects, atmospheric chemistry, and meteorology—is essential for the effective co-control of PM_{2.5} and
586 O₃ in the carbon neutrality era. Seasonally adaptive, region-specific, and chemically targeted policies are critical to maximizing
587 air quality and climate co-benefits under evolving environmental and policy contexts.

588 **Code availability**

589 The WRF-Chem model (version 3.7.1) used in this study is based on the standard release from NCAR
590 (<https://doi.org/10.5065/D6MK6B4K>), with modifications to the aerosol and chemical mechanisms. Details of these
591 modifications are documented in Section 2.2 of the paper. The updated code about model and NCL scripts used for data
592 processing and visualization can be provided upon request.

593 **Data availability**

594 The FNL (Final Analysis) meteorological data are available from the Research Data Archive of NCAR:
595 <http://rda.ucar.edu/datasets/ds083.2/>. The MEIC v1.4 emission inventory can be accessed at:
596 http://meicmodel.org/?page_id=560. Hourly surface O₃ observations are provided by the China National Environmental
597 Monitoring Centre (CNEMC) and are available at: <http://www.cnemc.cn/>.

598 **Author contributions**

599 **YL, and TW** formulated the research, and **YL**: carried it out. **ML, YQ, HW, and MX**: technical support on the WRF-Chem
600 model. **CL, YL, and YW**: reviewed the manuscript.

601 **Competing interests**

602 The corresponding author has stated that all the authors have no conflicts of interest.

603 **Disclaimer**

604 Publisher's note: Copernicus Publications remains neutral about jurisdictional claims in published maps and institutional
605 affiliations.

606 **Financial support**

607 This investigation was supported by the National Key Basic Research & Development Program of China (2024YFC3711905),
608 the Doctoral Scientific Research Fund of Henan Finance University (2024BS055), and the National Natural Science
609 Foundation of China (42477103), the Creative talent exchange program for foreign experts in the Belt and Road countries, the
610 Henan Provincial Science and Technology Research and Development Program (252102320085).

611 **References**

612 Brown, S. S. and Stutz, J.: Nighttime radical observations and chemistry, *Chem. Soc. Rev.*, 41, 6405-6447,
613 <https://doi.org/10.1039/C2CS35181A>, 2012.

614 Cao, J., Qiu, X., Liu, Y., Yan, X., Gao, J., and Peng, L.: Identifying the dominant driver of elevated surface ozone concentration
615 in North China plain during summertime 2012–2017, *Environ. Pollut.*, 300, 118912,
616 <https://doi.org/10.1016/j.envpol.2022.118912>, 2022.

617 Chen, J., Li, Z., Lv, M., Wang, Y., Wang, W., Zhang, Y., Wang, H., Yan, X., Sun, Y., and Cribb, M.: Aerosol hygroscopic growth,
618 contributing factors, and impact on haze events in a severely polluted region in northern China, *Atmos. Chem. Phys.*, 19,
619 1327-1342, <https://doi.org/10.5194/acp-19-1327-2019>, 2019.

620 Chen, X., Zhong, B., Huang, F., Wang, X., Sarkar, S., Jia, S., Deng, X., Chen, D., and Shao, M.: The role of natural factors in
621 constraining long-term tropospheric ozone trends over Southern China, *Atmos. Environ.*, 220, 117060,
622 <https://doi.org/10.1016/j.atmosenv.2019.117060>, 2020.

623 Cheng, J., Tong, D., Zhang, Q., Liu, Y., Lei, Y., Yan, G., Yan, L., Yu, S., Cui, R. Y., Clarke, L., Geng, G., Zheng, B., Zhang, X.,
624 Davis, S. J., and He, K.: Pathways of China's PM_{2.5} air quality 2015–2060 in the context of carbon neutrality, *Natl. Sci.
625 Rev.*, 8, <https://doi.org/10.1093/nsr/nwab078>, 2021.

626 Dai, H., Liao, H., Wang, Y., and Qian, J.: Co-occurrence of ozone and PM_{2.5} pollution in urban/non-urban areas in eastern
627 China from 2013 to 2020: Roles of meteorology and anthropogenic emissions, *Sci. Total Environ.*, 924, 171687,
628 <https://doi.org/10.1016/j.scitotenv.2024.171687>, 2024.

629 Dai, H., Liao, H., Li, K., Yue, X., Yang, Y., Zhu, J., Jin, J., Li, B., and Jiang, X.: Composited analyses of the chemical and
630 physical characteristics of co-polluted days by ozone and PM_{2.5} over 2013–2020 in the Beijing–Tianjin–Hebei region,
631 *Atmos. Chem. Phys.*, 23, 23-39, <https://doi.org/10.5194/acp-23-23-2023>, 2023.

632 Dang, R., Liao, H., and Fu, Y.: Quantifying the anthropogenic and meteorological influences on summertime surface ozone in
633 China over 2012–2017, *Sci. Total Environ.*, 754, 142394, <https://doi.org/10.1016/j.scitotenv.2020.142394>, 2021.

634 Dyson, J. E., Whalley, L. K., Slater, E. J., Woodward-Massey, R., Ye, C., Lee, J. D., Squires, F., Hopkins, J. R., Dunmore, R.
635 E., Shaw, M., Hamilton, J. F., Lewis, A. C., Worrall, S. D., Bacak, A., Mehra, A., Bannan, T. J., Coe, H., Percival, C. J.,
636 Ouyang, B., Hewitt, C. N., Jones, R. L., Crilley, L. R., Kramer, L. J., Acton, W. J. F., Bloss, W. J., Saksakulkrai, S., Xu,
637 J., Shi, Z., Harrison, R. M., Kotthaus, S., Grimmond, S., Sun, Y., Xu, W., Yue, S., Wei, L., Fu, P., Wang, X., Arnold, S. R.,
638 and Heard, D. E.: Impact of HO₂ aerosol uptake on radical levels and O₃ production during summertime in Beijing, *Atmos.
639 Chem. Phys.*, 23, 5679-5697, <https://doi.org/10.5194/acp-23-5679-2023>, 2023.

640 Gao, J., Zhu, B., Xiao, H., Kang, H., Pan, C., Wang, D., and Wang, H.: Effects of black carbon and boundary layer interaction
641 on surface ozone in Nanjing, China, *Atmos. Chem. Phys.*, 18, 7081-7094, <https://doi.org/10.5194/acp-18-7081-2018>,
642 2018.

643 Geng, G., Liu, Y., Liu, Y., Liu, S., Cheng, J., Yan, L., Wu, N., Hu, H., Tong, D., and Zheng, B.: Efficacy of China's clean air
644 actions to tackle PM_{2.5} pollution between 2013 and 2020, *Nat. Geosci.*, 17, 987-994, [https://doi.org/10.1038/s41561-024-01540-z](https://doi.org/10.1038/s41561-024-
645 01540-z), 2024.

646 George, C., Ammann, M., D'Anna, B., Donaldson, D. J., and Nizkorodov, S. A.: Heterogeneous Photochemistry in the
647 Atmosphere, *Chem. Rev.*, 115, 4218-4258, <https://doi.org/10.1021/cr500648z>, 2015.

648 Grell, G. A., Peckham, S. E., Schmitz, R., McKeen, S. A., Frost, G., Skamarock, W. C., and Eder, B.: Fully coupled “online”
649 chemistry within the WRF model, *Atmos. Environ.*, 39, 6957-6975, <https://doi.org/10.1016/j.atmosenv.2005.04.027>, 2005.

650 Guenther, A., Karl, T., Harley, P., Wiedinmyer, C., Palmer, P. I., and Geron, C.: Estimates of global terrestrial isoprene
651 emissions using MEGAN (Model of Emissions of Gases and Aerosols from Nature), *Atmos. Chem. Phys.*, 6, 3181-3210,
652 <https://doi.org/10.5194/acp-6-3181-2006>, 2006.

653 Hammer, M. U., Vogel, B., and Vogel, H.: Findings on H₂O₂/HNO₃ as an indicator of ozone sensitivity in Baden-Württemberg,
654 Berlin-Brandenburg, and the Po valley based on numerical simulations, *J. Geophys. Res.: Atmos.*, 107, LOP 3-1-LOP 3-
655 18, <https://doi.org/10.1029/2000JD000211>, 2002.

656 Hu, F., Xie, P., Xu, J., Lv, Y., Zhang, Z., Zheng, J., and Tian, X.: Long-term trends of ozone in the Yangtze River Delta, China:
657 spatiotemporal impacts of meteorological factors, local, and non-local emissions, *J. Environ. Sci.*, 156, 408-420,
658 <https://doi.org/10.1016/j.jes.2024.07.017>, 2025.

659 Jacob, D. J.: Heterogeneous chemistry and tropospheric ozone, *Atmos. Environ.*, 34, 2131-2159,
660 [https://doi.org/10.1016/S1352-2310\(99\)00462-8](https://doi.org/10.1016/S1352-2310(99)00462-8), 2000.

661 Jeon, W., Choi, Y., Souri, A. H., Roy, A., Diao, L., Pan, S., Lee, H. W., and Lee, S.-H.: Identification of chemical fingerprints
662 in long-range transport of burning induced upper tropospheric ozone from Colorado to the North Atlantic Ocean, *Sci.
663 Total Environ.*, 613-614, 820-828, <https://doi.org/10.1016/j.scitotenv.2017.09.177>, 2018.

664 Kong, L., Du, C., Zhanzakova, A., Cheng, T., Yang, X., Wang, L., Fu, H., Chen, J., and Zhang, S.: Trends in heterogeneous
665 aqueous reaction in continuous haze episodes in suburban Shanghai: An in-depth case study, *Sci. Total Environ.*, 634,
666 1192-1204, <https://doi.org/10.1016/j.scitotenv.2018.04.086>, 2018.

667 Li, J., Han, Z., Li, J., Liu, R., Wu, Y., Liang, L., and Zhang, R.: The formation and evolution of secondary organic aerosol
668 during haze events in Beijing in wintertime, *Sci. Total Environ.*, 703, 134937,
669 <https://doi.org/10.1016/j.scitotenv.2019.134937>, 2020a.

670 Li, K., Jacob, D. J., Liao, H., Shen, L., Zhang, Q., and Bates, K. H.: Anthropogenic drivers of 2013–2017 trends in summer
671 surface ozone in China, *Proceedings of the National Academy of Sciences*, 116, 422-427,
672 <https://doi.org/10.1073/pnas.1812168116>, 2019a.

673 Li, K., Jacob, D. J., Shen, L., Lu, X., De Smedt, I., and Liao, H.: Increases in surface ozone pollution in China from 2013 to
674 2019: anthropogenic and meteorological influences, *Atmos. Chem. Phys.*, 20, 11423-11433, <https://doi.org/10.5194/acp-20-11423-2020>, 2020b.

675 Li, M., Wang, T., Xie, M., Li, S., Zhuang, B., Chen, P., Huang, X., and Han, Y.: Agricultural Fire Impacts on Ozone
676 Photochemistry Over the Yangtze River Delta Region, East China, *J. Geophys. Res.: Atmos.*, 123, 6605-6623,
677 <https://doi.org/10.1029/2018JD028582>, 2018.

678 Li, M., Zhang, Q., Zheng, B., Tong, D., Lei, Y., Liu, F., Hong, C., Kang, S., Yan, L., Zhang, Y., Bo, Y., Su, H., Cheng, Y., and
679 He, K.: Persistent growth of anthropogenic non-methane volatile organic compound (NMVOC) emissions in China during
680 1990–2017: drivers, speciation and ozone formation potential, *Atmos. Chem. Phys.*, 19, 8897-8913,
681 <https://doi.org/10.5194/acp-19-8897-2019>, 2019b.

682 Li, Y., Wang, T., Wang, Q. g., Li, M., Qu, Y., Wu, H., and Xie, M.: Exploring the role of aerosol-ozone interactions on O₃ surge
683 and PM_{2.5} decline during the clean air action period in Eastern China 2014–2020, *Atmos. Res.*, 302, 107294,
684 <https://doi.org/10.1016/j.atmosres.2024.107294>, 2024a.

685 Li, Y., Wang, T., Wang, Q. g., Li, M., Qu, Y., Wu, H., and Xie, M.: Impact of aerosol-radiation interaction and heterogeneous
686 chemistry on the winter decreasing PM_{2.5} and increasing O₃ in Eastern China 2014–2020, *J. Environ. Sci.*, 151, 469-483,
687 <https://doi.org/10.1016/j.jes.2024.04.010>, 2025.

688 Li, Y., Wang, T., Wang, Q. g., Li, M., Qu, Y., Wu, H., Fan, J., Shao, M., and Xie, M.: Deciphering the seasonal dynamics of
689 multifaceted aerosol-ozone interplay: Implications for air quality management in Eastern China, *Sci. Total Environ.*, 946,
690 174327, <https://doi.org/10.1016/j.scitotenv.2024.174327>, 2024b.

691 Li, Y., Wang, T., Wang, Q. g., Qu, Y., Wu, H., Xie, M., Li, M., Li, S., and Zhuang, B.: Spatiotemporal Variations of PM_{2.5} and
692 O₃ Relationship during 2014–2021 in Eastern China, *Aerosol and Air Quality Research*, 23, 230060,
693 <https://doi.org/10.4209/aaqr.230060>, 2023.

694 Liu, H., Liu, S., Xue, B., Lv, Z., Meng, Z., Yang, X., Xue, T., Yu, Q., and He, K.: Ground-level ozone pollution and its health
695 impacts in China, *Atmos. Environ.*, 173, 223-230, <https://doi.org/10.1016/j.atmosenv.2017.11.014>, 2018.

696 Liu, Y. and Wang, T.: Worsening urban ozone pollution in China from 2013 to 2017 – Part 1: The complex and varying roles
697 of meteorology, *Atmos. Chem. Phys.*, 20, 6305-6321, <https://doi.org/10.5194/acp-20-6305-2020>, 2020.

698 Liu, Y., Geng, G., Cheng, J., Liu, Y., Xiao, Q., Liu, L., Shi, Q., Tong, D., He, K., and Zhang, Q.: Drivers of Increasing Ozone
699 during the Two Phases of Clean Air Actions in China 2013–2020, *Environ. Sci. Technol.*, 57, 8954-8964,
700 <https://doi.org/10.1021/acs.est.3c00054>, 2023a.

701 Liu, Z., Wang, H., Peng, Y., Zhang, W., Che, H., Zhang, Y., Liu, H., Wang, Y., Zhao, M., and Zhang, X.: The combined effects

703 of heterogeneous chemistry and aerosol-radiation interaction on severe haze simulation by atmospheric chemistry model
704 in Middle-Eastern China, *Atmos. Environ.*, 302, 119729, <https://doi.org/10.1016/j.atmosenv.2023.119729>, 2023b.

705 Lu, S., Gong, S., Chen, J., Zhang, L., Ke, H., Pan, W., Lu, J., and You, Y.: Contribution assessment of meteorology vs. emissions
706 in the summer ozone trend from 2014 to 2023 in China by an environmental meteorology index, *Atmos. Environ.*, 343,
707 120992, <https://doi.org/10.1016/j.atmosenv.2024.120992>, 2025.

708 Ma, D., Wang, T., Wu, H., Qu, Y., Liu, J., Liu, J., Li, S., Zhuang, B., Li, M., and Xie, M.: The effect of anthropogenic emission,
709 meteorological factors, and carbon dioxide on the surface ozone increase in China from 2008 to 2018 during the East
710 Asia summer monsoon season, *Atmos. Chem. Phys.*, 23, 6525-6544, <https://doi.org/10.5194/acp-23-6525-2023>, 2023a.

711 Ma, P., Quan, J., Dou, Y., Pan, Y., Liao, Z., Cheng, Z., Jia, X., Wang, Q., Zhan, J., Ma, W., Zheng, F., Wang, Y., Zhang, Y., Hua,
712 C., Yan, C., Kulmala, M., Liu, Y., Huang, X., Yuan, B., Brown, S. S., and Liu, Y.: Regime-Dependence of Nocturnal
713 Nitrate Formation via N_2O_5 Hydrolysis and Its Implication for Mitigating Nitrate Pollution, *Geophys. Res. Lett.*, 50,
714 e2023GL106183, <https://doi.org/10.1029/2023GL106183>, 2023b.

715 Ni, Y., Yang, Y., Wang, H., Li, H., Li, M., Wang, P., Li, K., and Liao, H.: Contrasting changes in ozone during 2019–2021
716 between eastern and the other regions of China attributed to anthropogenic emissions and meteorological conditions, *Sci.
717 Total Environ.*, 908, 168272, <https://doi.org/10.1016/j.scitotenv.2023.168272>, 2024.

718 Peng, Y.-P., Chen, K.-S., Wang, H.-K., Lai, C.-H., Lin, M.-H., and Lee, C.-H.: Applying model simulation and photochemical
719 indicators to evaluate ozone sensitivity in southern Taiwan, *J. Environ. Sci.*, 23, 790-797, [https://doi.org/10.1016/S1001-0742\(10\)60479-2](https://doi.org/10.1016/S1001-
720 0742(10)60479-2), 2011.

721 Qu, Y., Wang, T., Yuan, C., Wu, H., Gao, L., Huang, C., Li, Y., Li, M., and Xie, M.: The underlying mechanisms of $\text{PM}_{2.5}$ and
722 O_3 synergistic pollution in East China: Photochemical and heterogeneous interactions, *Sci. Total Environ.*, 873, 162434,
723 <https://doi.org/10.1016/j.scitotenv.2023.162434>, 2023.

724 Shao, M., Lv, S., Song, Y., Liu, R., and Dai, Q.: Disentangling the effects of meteorology and emissions from anthropogenic
725 and biogenic sources on the increased surface ozone in Eastern China, *Atmos. Res.*, 311, 107699,
726 <https://doi.org/10.1016/j.atmosres.2024.107699>, 2024.

727 Shao, M., Wang, W., Yuan, B., Parrish, D. D., Li, X., Lu, K., Wu, L., Wang, X., Mo, Z., Yang, S., Peng, Y., Kuang, Y., Chen,
728 W., Hu, M., Zeng, L., Su, H., Cheng, Y., Zheng, J., and Zhang, Y.: Quantifying the role of $\text{PM}_{2.5}$ dropping in variations of
729 ground-level ozone: Inter-comparison between Beijing and Los Angeles, *Sci. Total Environ.*, 788, 147712,
730 <https://doi.org/10.1016/j.scitotenv.2021.147712>, 2021.

731 Sun, L., Xue, L., Wang, Y., Li, L., Lin, J., Ni, R., Yan, Y., Chen, L., Li, J., and Zhang, Q.: Impacts of meteorology and emissions
732 on summertime surface ozone increases over central eastern China between 2003 and 2015, *Atmos. Chem. Phys.*, 19,
733 1455-1469, <https://doi.org/10.5194/acp-19-1455-2019>, 2019.

734 Wu, K., Wang, Y., Qiao, Y., Liu, Y., Wang, S., Yang, X., Wang, H., Lu, Y., Zhang, X., and Lei, Y.: Drivers of 2013–2020 ozone
735 trends in the Sichuan Basin, China: Impacts of meteorology and precursor emission changes, *Environ. Pollut.*, 300,
736 118914, <https://doi.org/10.1016/j.envpol.2022.118914>, 2022.

737 Yan, D., Jin, Z., Zhou, Y., Li, M., Zhang, Z., Wang, T., Zhuang, B., Li, S., and Xie, M.: Anthropogenically and meteorologically
738 modulated summertime ozone trends and their health implications since China's clean air actions, *Environ. Pollut.*, 343,
739 123234, <https://doi.org/10.1016/j.envpol.2023.123234>, 2024.

740 Yang, H., Chen, L., Liao, H., Zhu, J., Wang, W., and Li, X.: Weakened aerosol–radiation interaction exacerbating ozone
741 pollution in eastern China since China's clean air actions, *Atmos. Chem. Phys.*, 24, 4001-4015,
742 <https://doi.org/10.5194/acp-24-4001-2024>, 2024.

743 Yang, L., Luo, H., Yuan, Z., Zheng, J., Huang, Z., Li, C., Lin, X., Louie, P. K. K., Chen, D., and Bian, Y.: Quantitative impacts
744 of meteorology and precursor emission changes on the long-term trend of ambient ozone over the Pearl River Delta,
745 China, and implications for ozone control strategy, *Atmos. Chem. Phys.*, 19, 12901-12916, [https://doi.org/10.5194/acp-19-12901-2019](https://doi.org/10.5194/acp-
746 19-12901-2019), 2019.

747 Yin, H., Lu, X., Sun, Y., Li, K., Gao, M., Zheng, B., and Liu, C.: Unprecedented decline in summertime surface ozone over
748 eastern China in 2020 comparably attributable to anthropogenic emission reductions and meteorology, *Environ. Res. Lett.*,
749 16, 124069, <https://doi.org/10.1088/1748-9326/ac3e22>, 2021.

750 Yu, C., Huang, L., Xue, L., Shen, H., Li, Z., Zhao, M., Yang, J., Zhang, Y., Li, H., Mu, J., and Wang, W.: Photoenhanced
751 Heterogeneous Uptake of NO₂ and HONO Formation on Authentic Winter Time Urban Grime, *ACS Earth Space Chem.*,
752 6, 1960-1968, <https://pubs.acs.org/doi/10.1021/acsearthspacechem.2c00054>, 2022.

753 Yu, Y., Wang, Z., He, T., Meng, X., Xie, S., and Yu, H.: Driving factors of the significant increase in surface ozone in the
754 Yangtze River Delta, China, during 2013–2017, *Atmos. Pollut. Res.*, 10, 1357-1364,
755 <https://doi.org/10.1016/j.apr.2019.03.010>, 2019.

756 Zhai, S., Jacob, D. J., Wang, X., Shen, L., Li, K., Zhang, Y., Gui, K., Zhao, T., and Liao, H.: Fine particulate matter (PM_{2.5})
757 trends in China, 2013–2018: Separating contributions from anthropogenic emissions and meteorology, *Atmos. Chem.*
758 *Phys.*, 19, 11031-11041, <https://doi.org/10.5194/acp-19-11031-2019>, 2019.

759 Zhang, H., Roehl, C. M., Sander, S. P., and Wennberg, P. O.: Intensity of the second and third OH overtones of H₂O₂, HNO₃,
760 and HO₂NO₂, *J. Geophys. Res.: Atmos.*, 105, 14593-14598, <https://doi.org/10.1029/2000JD900118>, 2000.

761 Zhang, X., Zhang, W.-C., Wu, W., and Liu, H.-B.: Understanding ozone variability in spatial responses to emissions and
762 meteorology in China using interpretable machine learning, *iScience*, 28, 113036,
763 <https://doi.org/10.1016/j.isci.2025.113036>, 2025.

764 Zhao, X., Zhang, Z., Xu, J., Gao, J., Cheng, S., Zhao, X., Xia, X., and Hu, B.: Impacts of aerosol direct effects on PM_{2.5} and
765 O₃ respond to the reductions of different primary emissions in Beijing-Tianjin-Hebei and surrounding area, *Atmos.*
766 *Environ.*, 309, 119948, <https://doi.org/10.1016/j.atmosenv.2023.119948>, 2023.

767 Zhou, M., Zhang, L., Chen, D., Gu, Y., Fu, T.-M., Gao, M., Zhao, Y., Lu, X., and Zhao, B.: The impact of aerosol–radiation
768 interactions on the effectiveness of emission control measures, *Environ. Res. Lett.*, 14, 024002,
769 <https://doi.org/10.1088/1748-9326/aaf27d>, 2019.

770 Zhu, J., Chen, L., Liao, H., Yang, H., Yang, Y., and Yue, X.: Enhanced PM_{2.5} Decreases and O₃ Increases in China During
771 COVID-19 Lockdown by Aerosol-Radiation Feedback, *Geophys. Res. Lett.*, 48, e2020GL090260,
772 <https://doi.org/10.1029/2020GL090260>, 2021.

773